Orbital Tracking of an Asteroid with a Phased Array of Radio Transponders

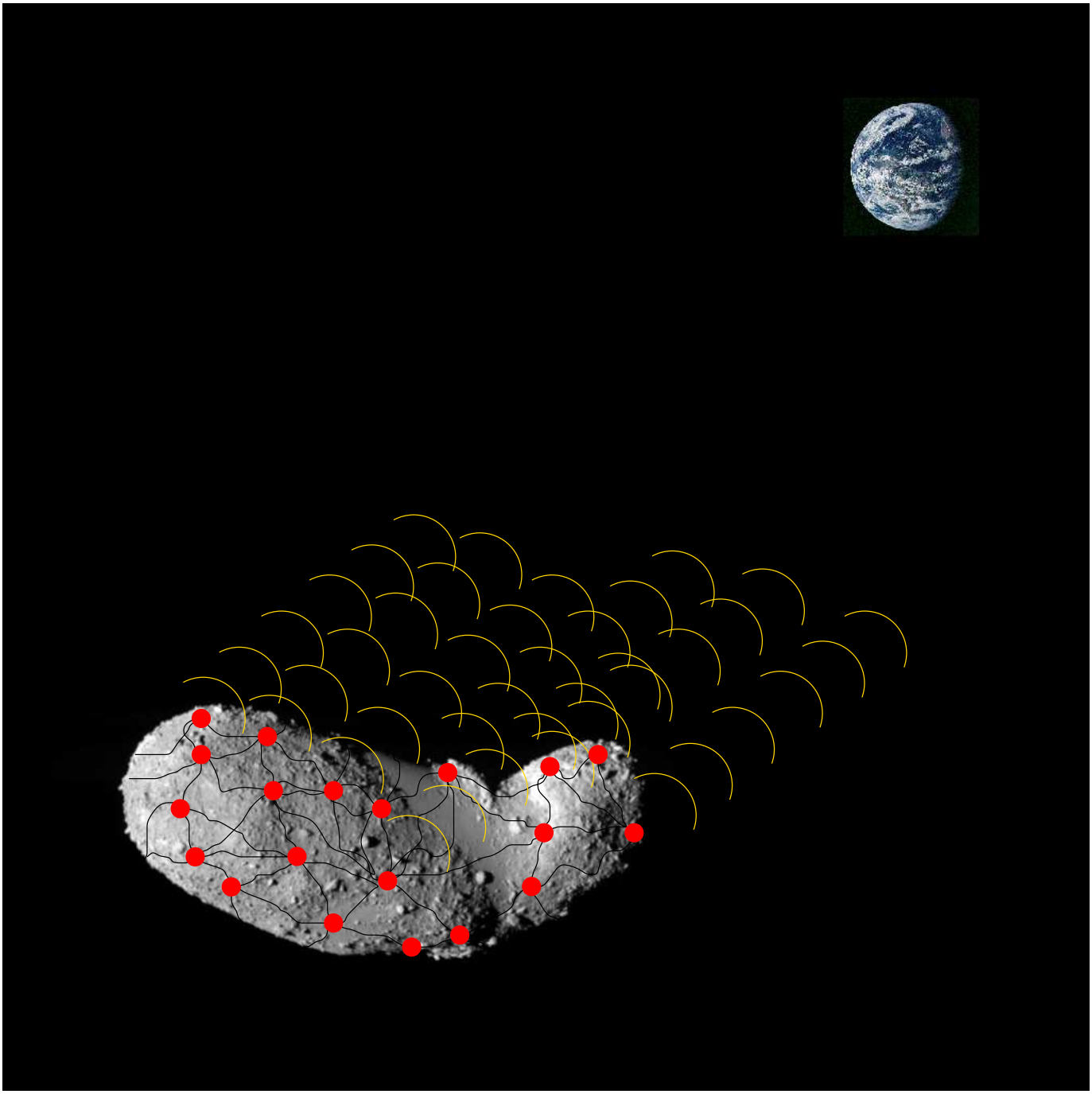

Image credits: Asteroid Itokawa: JAXA [1], Earth: NASA [2]

Orbital Tracking of an Asteroid with a Phased Array of Radio Transponders

Bernhard W. Adams

bernhard@bernhard-adams.com

December 27, 2010

1 Executive Summary

A novel way is suggested of tracking an asteroid's orbit to determine the danger it may pose to earth. It is based upon the idea of linking many small radio transponders on the asteroid to a phased array that maintains a radio link with the earth without mechanical motion. The main challenges in a tracking mission are due to the limitations in power and in deliverable payload, as well as the low surface gravity of the asteroid. These are solved here through state-of-the-art GPS and cell-phone technology with adaptations to the space environment.

A web of 800 m diameter links 475 transponders with multiple antennas each, and provides mechanical and electrical connections, as well as optical-fiber communication. It is made to collide gently with the asteroid, and gets entangled with it, so the transponders cannot bounce off and escape. After some time the transponders settle down in fixed random locations. They then receive a calibration radio signal from the earth, and compare phases through the optical-fiber-communication network. Doing so throughout one rotation period of the asteroid, they determine their locations on it. This phase relationship is then used directly for reception from the earth, and is inverted for transmission. If some of the transponders are damaged during landing the array will still work at slightly degraded performance. Electric power for the electronics is provided through solar cells, and is shared through the electrical connections in the web.

This approach is robust through a high inherent redundancy, which can optionally be enhanced further by independently sending multiple fiber-linked arrays to the asteroid, and having them link up to one single array by in-situ low-power radio communication.

The tracking accuracy is 1 μm/s for the velocity and 5 m for the distance throughout most of the asteroid's orbit. The payload to reach the asteroid is about 70 kg to deposit on the asteroid plus 80 kg for the delivery spacecraft. This is well within the capabilities of available rocket technology.

Keywords: phased array; web for multiple purposes: landing, electrical power distribution, and optical-fiber communication for array phasing; redundancy on multiple levels; ranging to 5 m, velocity accuracy of 1 μm/s

2 Introduction

Asteroids with orbits crossing that of the earth pose a danger of low probability, but possibly devastating consequences [3]. They are generally of rocky composition, but details are unclear, such as whether they are solid chunks or piles of rubble. Sizes can range from meters to hundreds of meters, larger ones presumably discovered long ago and ruled out as threats. Impact velocities range from about 12 km/s to about 80 km/s, i.e., from slightly larger than earth's escape velocity for an object co-orbiting the sun with the earth to a head-on collision in counter-directed orbits about the sun.[1] Co-orbiting asteroids are much more likely to hit the earth than counter-orbiting ones because most celestial bodies in the solar system follow the motion of the original accretion disk that formed it. Furthermore, the phenomenon of "resonant returns" [4] tends to lock the orbital periods of near-earth asteroids into resonance, where the asteroid completes n orbital periods for m of the earth.

One such potentially dangerous object is Apophis, a rock between 250 and 400 meters in size [5], orbiting the sun in 323 days. An impact at about 12.59 km/s [6] would release an estimated equivalent of about 400 mega-tons of TNT, comparable to the Krakatoa eruption of 1883. Apophis will pass very close to the earth in 2029. Although an impact in that year has now been ruled out through telescopic and radar measurements, earth's gravitational pull may set it up for one in 2036. This will happen if the asteroid passes through a small 600-meter-wide region in space called the "keyhole" [7], which is much easier to avoid than the entire earth. Therefore, if a deflection becomes necessary, it should be done before 2029. The minimum amount of velocity change for missing the keyhole oscillates slightly along Apophis' orbit, and increases slowly towards 2029 (fig. 2 of ref. [8]). Up to about 2026, less than 10^{-6} m/s along the orbital path are sufficient, but after passage through the keyhole center the required velocity change exceeds 10^{-2} m/s [8]. Given the estimated mass of $2.1 \cdot 10^{10}$ kg [6], the smaller velocity change of 10^{-6} m/s can be achieved by means like an impact of a 1000-kg mass [5], or a rocket-driven "tugboat" [9, 10], a gravity tractor [11], or a rock-slinging catapult (see app. D), etc. These means appear insufficient after 2029, probably leaving only the unappealing option of a nuclear explosion.

Accurate orbital tracking is required to determine whether a deflection becomes necessary, and this needs to be done right up to the 2029 encounter because the Yarkovski effect [5, 12] introduces non-negligible perturbations. Passive radar, i.e., reflection of radar pulses off the asteroid is typically accurate to within tens of meters in range and centimeters per second in velocity [13] (down to 0.1 mm/s for very close approaches [14]). Furthermore, its range is limited to about 0.14 astronomical units (AU)) with the 70-meter Goldstone antenna and 0.3 AU for the much less steerable Arecibo antenna [5]. A radio transponder on the asteroid can greatly enhance the accuracy and range.

The following text is structured to first pose design goals and challenges (sec. 3), leading to basic design decisions (sec. 4), which are then discussed in detail (sec. 5).

[1] Comets coming from far out are much less likely to hit the earth, but are harder to detect or deflect.

3 Design Goals and Challenges

Corresponding to the velocity change required to make the asteroid miss the keyhole, the design goal of the mission is an accuracy of 10^{-6} m/s in velocity and 5 m in distance (corresponding to 10^{-6} m/s in about two months) for most of the asteroid's orbit. The main challenges are:

- payload limitations
- limitations in power for the radio transmitters
- alternating exposure of the transponders to sunlight and shadow with consequences for power supply and thermal management
- maintaining radio directionality towards the earth from the rotating asteroid
- spectral broadening of radio signals passing through the plasma of the ionosphere and interplanetary space (scintillations)
- the unknown surface composition and the low gravity
- the harsh space environment, such as energetic solar protons

Accuracy, scintillations, and the gravity of the asteroid are discussed in more detail, below, and solutions to the challenges are discussed in sec. 4.

3.1 Accuracy

To avoid an unnecessarily strong deflection, the accuracy of the orbit determination should reflect the maximum required pre-keyhole velocity change of $1 \cdot 10^{-6}$ m/s tangential to the asteroid's orbit. Repeated measurements are often used for orbital refinement, but the present application would benefit from the full accuracy in each single measurement (as defined in secs. 5.1.2 and 5.4) through the capabilities of a) live monitoring the effect of a deflection, and b) correcting for deviations from a purely celestial-mechanical orbit due to the Yarkowski effect [5, 12].
Therefore, the accuracy goals of this proposal are 10^{-6} m/s for Doppler-based determination of the radial velocity $\mathbf{v}_r$ relative to earth (fig. 1), and 5 meters in ranging (corresponding to 10^{-6} m/s over two months, i.e., 1/4 of the orbital period). These accuracies are stipulated for all of the asteroid's orbit, except an angle of $\pm 30°$ from the earth-to-sun direction (fig. 1), within which the proximity of the line-of-sight to the sun leads to excessive radio-signal degradation by plasma scintillation in the solar wind. With the asteroid at aphelion and the earth 30° degrees from opposition to it, the earth-to-asteroid distance is maximum at 1.82 A.U. ($2.72 \cdot 10^8$ km), and the line-of-sight passes at 0.5 A.U. (107 solar radii) from the sun.
Passive radar is accurate [13] to centimeters per second and tens of meters in distance, which is insufficient for the present purpose. Therefore, one or more transponders must be attached to the asteroid, either by landing, or by placing a spacecraft into orbit around it. The latter option is problematic, as discussed in sec. 3.2.

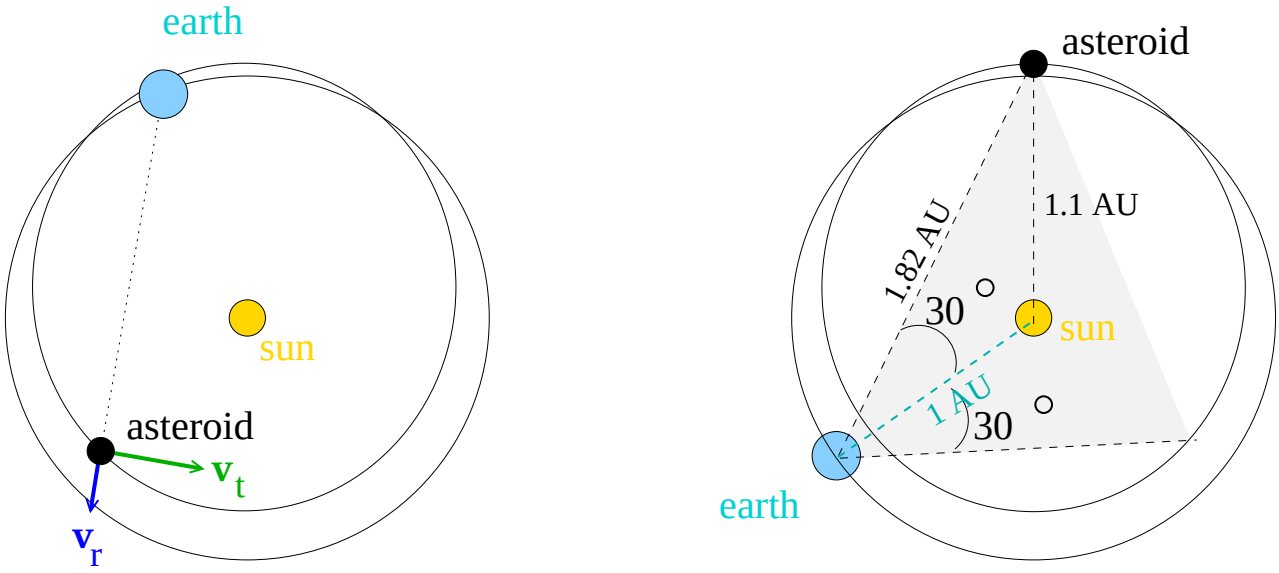

Figure 1: The design goals are a Doppler accuracy of 10^{-6} m/s for the radial velocity $\mathbf{v}_r$ and a ranging accuracy of 5 m for most of the asteroid's orbit, except for an angle of $\pm 30°$ from opposition to the earth (the shaded area, see also fig. 15). The maximum earth-to-asteroid distance is 1.82 A.U.

For lack of angular resolution, even with very-long-baseline interferometry (VLBI), the velocity component $\mathbf{v}_t$ transverse to the line-of-sight cannot be measured at the same level of accuracy as $\mathbf{v}_r$, but it can be deduced from celestial mechanics and radar measurements when the line-of-sight is tangential to the asteroid's orbit in 2014 (fig. 17).
For the stipulated precision of $\Delta v = 10^{-6}$ m/s of the Doppler measurements, the transponder radio frequency must be stable within $\Delta v/c = 3 \cdot 10^{-15}$ relative to an earth-based clock, where c is the speed of light. This can be achieved with a coherent link, where the radio signal from the spacecraft is phase-locked to one sent from the earth, as was first demonstrated with the Mariner 10 spacecraft [15]. A slight variation of the technique is proposed here (sec. 5.1.2). Interplanetary-plasma scintillations (see sec. 3.3) can be compensated using multiple coherently locked frequencies, as has been demonstrated with about $5 \cdot 10^{-7}$ m/s accuracy in the gravitational-wave experiment on the Cassini spacecraft currently orbiting Saturn [16].

3.2 Gravity of the Asteroid, Orbiting

With an estimated mass of about $M = 2.1 \cdot 10^{10}$ kg [6], Apophis exerts a very weak gravitational pull, thus posing unique challenges in landing. For a spherical homogeneous body of this mass the gravitational acceleration a at a distance r from the center is given by $a = \gamma M/r^2$, where $\gamma = 6.67300 \cdot 10^{-11} m^3 kg^{-1} s^{-2}$ is the gravitational constant. Thus, an estimate for the surface gravity is $a = 4.4 \cdot 10^{-5} m/s^2$ at $r = 150$ m. The actual shape of the asteroid is irregular, so the the gravitational acceleration is generally not directed along the surface normal.
The escape velocity is given by

$$v_e = \sqrt{\frac{2\gamma M}{r}} \tag{1}$$

which comes to be 9.7 cm/s on a sphere at $r = 150$ m, but the irregular shape makes the escape velocity location-dependent. A lander that bounces off faster than v_e will not return to the asteroid. The period T of a satellite orbiting a sphere of isotropic mass distribution at a distance R from its center is given by Kepler's law

$$\frac{T^2}{R^3} = \frac{4\pi^2}{\gamma M} \tag{2}$$

With the mass of Apophis and an orbital radius of $R = 300$ m, the period is $T = 27580$ s, or a little over 7 1/2 hours at an orbital velocity of $2\pi R/T = 6.8$ cm/s. This gives a rough estimate of the timescales for the transponders to come to rest after "impacting" and rebounding a few times.
However, due to the irregular shape of the asteroid, an actual orbit is not elliptic, and generally not periodic. This would, however, be necessary to be able to deduce the asteroid's velocity from that of the orbiter. Sophisticated methods exist to determine periodic orbits about bodies of iregular shape [17, 18], but the problem is compounded by the asteroid's rotation. A possible solution would be to choose an orbit within the equatorial plane (through the center of mass and perpendicular to the rotation axis) with the same period as that of the rotation (like a geostationary orbit). Given the unknown shape and mass distribution of the asteroid, such an orbit will be very hard to find.

3.3 Scintillations

Radio waves experience refraction and attenuation in the earth's atmosphere and in interplanetary space. Variations in the refractive index introduce radio phase fluctuations known as scintillations. The resulting spectral broadening degrades the accuracy of Doppler-based velocity measurements [19] and increases the signal bandwidth, thus requiring a higher transmitter power to overcome the noise threshold. Refraction occurs in the troposphere, the earth's ionosphere, and in the solar-wind plasma of interplanetary space.
Tropospheric radio refraction is mainly due to water vapor, and exhibits almost no frequency dispersion up to about 30 GHz. Scintillations can be modeled by wind-driven regions of varying moisture content moving across the line-of-sight. Radio-telescopic measurements taken at 5 GHz [20] indicate an Allen variance of the phase of about 10^{-15} at 1000-second integration intervals (commensurate with the phase-slippage update rate (see sec. 5.1.4). Tropospheric density variations can be measured independently of the radio signals, and can thus be compensated [19].
Now to the plasma of the ionosphere and of interplanetary space: At frequencies ω high above the plasma frequency $\omega_p = \sqrt{4\pi\rho c^2 r_e}$ (which is the case for GHz frequencies in the ionosphere ($\rho = 10^4 \ldots 10^6 \mathrm{cm}^{-3}$) and in interplanetary space ($\rho \approx 10 \mathrm{cm}^{-3}$ at 1 A.U.)), the refractive index of a conductive medium is [21], sec. 7.5:

$$n \approx 1 - \frac{1}{2}\frac{\omega_p^2}{\omega^2} = 1 - \frac{2\pi c^2 r_e \rho}{\omega^2} \tag{3}$$

where ρ is the electron density, c is the speed of light and $r_e = 2.82 \cdot 10^{-13}$ cm is the classical electron radius. Due to the linear dependence on ρ the optical path L_o relative to vacuum is proportional to the total electron content (TEC) obtained by integrating along a ray path, and the phase retardation is L_o/λ

$$\phi_r = \frac{c r_e}{\omega} \int \rho ds \tag{4}$$

Ionospheric scintillations depend on the time of day and the solar activity. They are well-known for their effect on the accuray of GPS.
Interplanetary-plasma scintillations have been studied through direct plasma-density measurements and their effect on radio communication with space probes from Pioneer 6 [22] to Cassini [23]. A widely used model assumes clouds of plasma passing through the line-of-sight at the velocity of the solar wind. According to the Kolmogorov theory of turbulence the spatial power spectrum of the plasma density has a power-law dependence on its wave vector $\mathbf{K}$ with an exponent $q = -11/3$. This leads [22, 24, 25] to a power law with exponent $q-2$ for the frequency of the amount of charge carried by the solar wind past by a stationary observer, and to a power law of ν^{q-1} for the power spectrum $P(\nu)$ of the scintillation-induced deviations ν from the transmitter frequency. Observations [15, 26] give $\nu^{-2.6}$ for the scintillation power spectrum in good agreement with the Kolmogorov exponent of $q = 11/3$. The bandwidth B of the spectral broadening is related to the power spectrum through (eq. (38) of ref. [22])

$$\int_0^{B/2} P(\nu)d\nu = \frac{1}{2}\int_0^{\infty} P(\nu)d\nu \tag{5}$$

As the outgoing solar wind expands, its effect on the refractive-index fluctuations decreases. For lines-of-sight between transmitter and receiver that pass by more than 10 solar radii $R_\odot$ from the sun (fig. 3.3) the variance σ of the scintillation broadening is well described by a power law with $\sigma \sim R^{-1.3}$ [26] (note: by the Wiener-Khitchine theorem, the spectral power density $P(\nu)$ is given by the autocorrelation of the spectrum, so σ^2 is proportional to $P(\nu)$ (see also eq. (10) of ref. [26]), and $P(\nu)$ goes as $R^{-2.6}$). The bandwidth B is found in ref. [26] to go as $B \sim \sigma^{6/5}$, so $B \sim R^{-1.6}$.

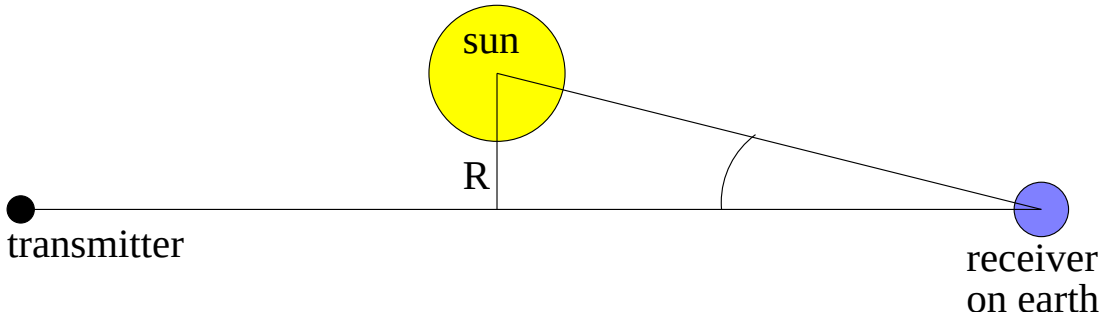

Figure 2: Geometry of the line-of-sight, adapted from fig. 7 of ref. [26].

Data on scintillations in radio signals are available from several space missions. The Helios 1 and 2 spacecraft [26] moved between 1/2 and 1 A.U. from the sun with the line-of-sight passing within $R = 1R_\odot$ and $R = 40R_\odot$ from the sun. Extrapolating these data to $107R_\odot$ (see sec. 3.1) gives a bandwidth of less than 0.1 Hz for signals of 2.3 GHz. The phase variations of radio signals go with $1/\omega$ (eq. (4)), so the bandwidth of scintillations at a higher radio frequency of, say, 8 GHz is proportionally reduced to several 10^{-2} Hz. Solar events may, however, considerably increase this broadening. An example is shown in fig. 9 of ref. [19].

4 Overview of the Proposed Solution

The solution of the present proposal will now be found by reviewing the challenges posed in sec. 3, and making basic design decisions. These leads to more specific challenges to be answered in sec. 5.

Landing vs. orbiting: Given the problems with deducing the asteroid's velocity from that of a transponder in an irregular orbit around it (see sec. 3.2), such a solution appears unappealing. That leaves the option of landing on the asteroid one or several transponders, either for direct communication with the earth, or through a relay satellite orbiting the asteroid. This proposal will focus on direct communication.

Staying put: Landing on the low-gravity surface without bouncing off at escape velocity is difficult [27]. The Rosetta cometary mission will solve this problem by shooting harpoons into the comet body [28], but this is not an option on the rocky surface of the asteroid. One might consider shaped explosive charges to create anchoring holes, but this would require solid rock, which is uncertain. One might also consider using an adhesive, but the unknown surface composition makes this also very risky. This leads to one of the central ideas of this proposal, which is to gently (<1 m/s) collide the asteroid with a large cobweb-like net, about 800 meters in diameter, and entangle it in the process. Transponders attached to the web may initially bounce off the asteroid in slow-motion, but will be restrained to eventually settle down.
Photoelectron emission from the asteroid under solar UV irradiation may lead to electrostatic repulsion of the transponders that may overcome gravity. This is discussed further in sec. 5.2.

Directionality, antenna gain: To operate with limited power, the transponder must have a high antenna gain. Spacecraft normally use dish antennas or printed dipole arrays. However, the rotation of the asteroid requires the antenna to track the direction towards the earth, adding mechanical complexity not found in attitude-controlled spacecraft. Furthermore, stabilizing the base of a mechanically tracking antenna is difficult in the low surface gravity of the asteroid. A much better alternative is a phased array where many antennas transmit and receive with an electronically controlled mutual phase relationship that provides constructive interference in the intended direction. A phased array with N dipoles spaced by more than a wavelength and driven to the same amplitude has a gain of N (i.e., $(10 \cdot \log_{10} N)$ dBi) over the individual antennas [29], regardless of the array regularity. If the antennas have uniformly random orientations, the gain is reduced by a factor of 4 (6 dBi) (see app. C).
A distributed antenna array with decentralized electronics is highly compatible with the web used for landing. Initially, the locations of the transponders on the asteroid, and thus the required phases, are unknown. Each transponder now relates the received phase of a calibration radio signal sent from earth to a reference distributed through the fiber-optic network throughout one rotation period of the asteroid. By communicating through the fibers and comparing the phases, the transponders can find their locations on the asteroid, and determine phase relationships for reception and transmission. One might also consider using low-power local radio communication for the reference signal, but the surface topography of the asteroid makes radio communication difficult, and the initially unknown

distances between the transponders introduce initially unknown phase offsets in the reference, greatly compounding the problem of finding the locations of the transponders.

Choice of Frequencies: To minimize scintillations in the Doppler measurements, a high frequency should be chosen. With recent advances in monolithic microwave integrated circuits (MMIC), lightweight microwave technology is now available for the X and Ku bands (8 to 18 GHz) [30]. Even so, at least two frequencies are required to achieve the stipulated accuracy of 10^{-6} m/s for relatively short integration times of about 1000 s (see app.B). The situation is different for ranging, where the intrinsic signal bandwidth makes scintillations irrelevant, but sophisticated modulation schemes and relatively large RF powers are required. This is best achieved with wireless (cell-phone, bluetooth, etc.) technology using frequencies between 900 MHz and 2.4 GHz. A secondary, non-technical reason for using cell-phone-compatible technology is that this may make the project attractive for sponsoring by cell-phone manufacturers (see app. F).

Power Supply: Spacecraft operating at earth-like distances from the sun are often powered by solar cells. However, other than in a free-flying spacecraft, transponders on the rotating asteroid receive only intermittent sunlight. Buffer batteries are not a good option because they would have to bridge several hours of shade for most transponders, and occasionally months near the spin axis. Radioisotope generators (RTGs) could provide uninterrupted power, but lightweight RTGs for powering the distributed electronics of the array have not been tested in space. Furthermore, RTGs are risky to launch, and public acceptance of radioactive sources on a body that might collide with the earth is problematic. Luckily, the distributed nature of the array offers another possibility, where the links between the transponders contain thin metal/carbon wires that provide electrical connections. These are switched dynamically to establish time-varying current paths reaching each transponder at least some of the time. Thus, transponders in the sunlight provide power to those in the shade, and the network adapts itself to the variable illumination.

Summary: The above considerations lead to the following solution: Land 475 transponders, each with 24 antennas for each radio channel, on the surface of the asteroid, using a web to avoid bouncing off. The transponders link up to a phased array that tracks the direction towards the earth while the asteroid is rotating. The web also distributes solar-generated power from parts in the sunlight to those in the shade, dynamically adjusting to the rotation of the asteroid. The radio technology resembles that of cell phones, but is adapted to the space environment, particularly regarding the radiation tolerance.

5 Details

5.1 Radio Signals

Radio signals to/from the asteroid serve the multiple purposes of initial phasing of the array, Doppler-based velocity determination, ranging, and digital communication. These functions are served here by separate carrier frequencies denoted as $\nu_{ddi}, i = 1, 2$ for two Doppler carriers (see app. B), and

ν_{dr}, ν_{dc} for ranging and communication carriers in the downlink (asteroid to earth), and $\nu_{udi}, \nu_{ur}, \nu_{uc}$ for the same functions in the uplink. Phasing of the array, i.e., the initial determination of the transponder locations, as well as subsequent continuous refinement, is done using the uplink Doppler signal. For reasons given above, the Doppler carriers lie in the high-frequency X and Ku bands, while the ranging and communication carriers are in the lower-frequency S band. For the purposes of this discussion, the frequencies listed in Table 1 will be chosen, but the final choice may be different, depending on technical details and on finding a good fit in the radio allocation chart [31] (U.S., and international).

carrier	frequency	purpose	assigned to
ν_{dd1}	8.400 GHz	downlink Doppler 1	space research
ν_{dd2}	16.800 GHz	downlink Doppler 2	space research
ν_{ud1}	8.484 GHz	uplink Doppler 1	space research
ν_{ud2}	16.968 GHz	uplink Doppler 2	space research
ν_{dr}	2250 ± 10 MHz	downlink ranging	space operations
ν_{ur}	2100 ± 10 MHz	uplink ranging	space operations
ν_{dc}	1.25 GHz	downlink communication	amateur radio
ν_{uc}	1.27 GHz	uplink communication	amateur radio

Table 1: Carrier frequencies exemplarily chosen for this proposal.

5.1.1 Initial Phasing of the Array

Right after placement in initially unknown locations on the asteroid, the transponders do not yet form an array. To determine their locations, a signal is sent from earth at the Doppler uplink frequency ν_{ud1} of 8.484 GHz. The receivers in the transponders must monitor a frequency bandwidth for this signal, which is dominated by the initial uncertainty δv of the asteroid's radial velocity relative to the earth (contributing about 30 Hz at $\delta v = 1$ m/s and $\nu_{ud} = 8.484$ GHz). Other, smaller contributions to this bandwidth are scintillation broadening of typically less than 0.1 Hz (sec. 3.3), and the spread of radial velocities due to the asteroid's rotation (about 1 turn in 30.5 hours [32], leading to a maximum velocity of 0.01 m/s at a distance of 200 m from the rotation axis). As with all radio signals, this bandwidth determines the minimum required transmitter power (calculated in sec. 5.3).

5.1.2 Doppler Measurements

To achieve the stipulated Doppler accuracy of 10^{-6} m/s, a variation of a coherent link is used. In the standard implementation of this technique, a radio signal sent from the earth is repeated phase-coherently by a transponder on a spacecraft, and the phase of this returned signal is compared with the one sent out. A coherent two-frequency link on the Cassini spacecraft has achieved a radial-velocity accuracy better than 1 μm/s [33]. Two frequencies will also be used here for reasons discussed in app. B.

Given the distributed nature of the transponder array and the variable exposure to sunlight, phase-locking a local oscillator to a radio signal from the earth may be difficult. Therefore, a variation of the coherent link is proposed, where the signal from a compact free-running atomic clock on the asteroid is mixed with a radio signal from the earth, and the accumulated phase slippage (time integral of the beat frequency) is transmitted to the earth through the digital communication link. Likewise, phase slippages are recorded on the earth end of the link. This leads to a quadratic equation that yields the radial velocity of the asteroid (see fig. 3 and app. A). Recently developed wristwatch-size clocks with an Allen variance of better than 10^{-10} in 1000 s [34] can keep the phase slippage down to a few times 2π per second, so that the amount of transmitted data is rather limited.
This modified coherent-link technique is illustrated in fig. 3 for a single Doppler carrier. An atomic-

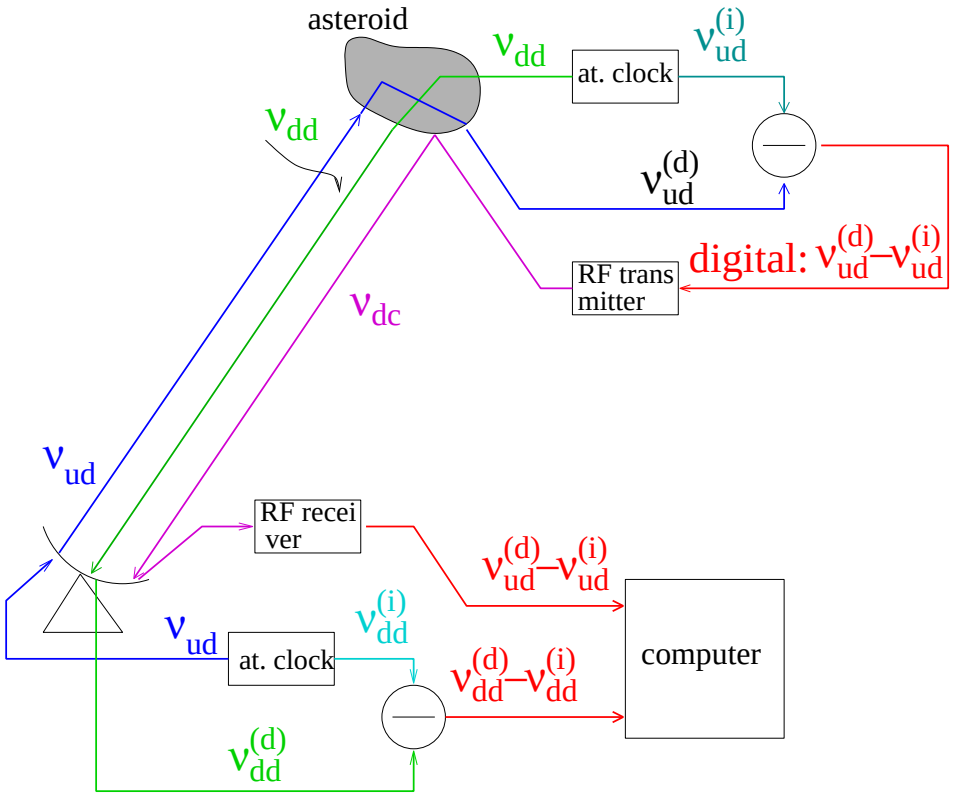

Figure 3: Modified coherent link: Frequencies derived from free-running atomic clocks on the ground and on the asteroid are transmitted, and are compared on both sides. The phase slippage measured on the asteroid is transmitted to the ground for camparison with the one measured there.

clock-stable signal of frequency ν_{ud} is sent from the earth to the asteroid. Due to the Doppler shift a slightly different frequency $\nu_{ud}^{(d)}$, and is subtracted inside the transponder from another, $\nu_{ud}^{(i)}$ that is derived from the on-board atomic clocks. Within the stability of the on-board atomic clock, $\nu_{ud}^{(i)} = \nu_{ud}$. The difference $\nu_{ud}^{(d)} - \nu_{ud}^{(i)}$ leads to the accumulation of a phase slippage $\phi_{ud} = (\nu_{ud}^{(d)} - \nu_{ud}^{(i)})\tau_{ud}$ over a time interval τ_{ud}, and is transmitted periodically (such as once in τ_{ud}) to the ground station by way of the digital communication link (below). Due to the stability of the on-board atomic clocks, these transmissions need occur only once per coherence time interval $\tau_c = 1/(\sigma\nu_{dd})$ of the carrier

frequency ν_{dd}, i.e., $\tau_{ud} = \tau_c$ (100s with $\nu_{dd} = 1$ GHz and $\sigma = 10^{-11}$). Another signal of frequency ν_{dd} derived from the same on-board atomic clock is transmitted to the earth, and is received there as $\nu_{dd}^{(d)}$. It is compared on the ground to a frequency $\nu_{dd}^{(i)}$, nominally equal to ν_{dd} derived from the ground-based master clock. The phase slippage of these two signals is then compared to the one measured on the asteroid and transmitted through the digital communication channel. This leads to a quadratic equation from which the radial velocity v_r is determined (app. A). For a velocity resolution of 1μm/s with a carrier frequency of 8 GHz a Doppler shift of $\Delta\nu = 2.7 \cdot 10^{-5}$ Hz must be measured. This takes an integration time of 520 s for a detectable radiofrequency phase difference of 5°.

5.1.3 Ranging

Similarly to GPS ranging, a signal of frequency ν_{ur} in the uplink is modulated with a pseudo-random code (PRN) through phase-shift keying (PSK). As in GSM cell phones, Gaussian Minimum-Shift Keying (GMSK) is used here for optimum spectral efficiency (in GSM the bit-time-bandwidth product is BT=0.3 [35], p. 1-9). For a maximum bit-error-rate (BER) of 10^{-3}, the signal-to-noise ratio (SNR) must then be about 20 dB (see fig. 10b in ref. [36]), in agreement with the GSM specification [37]. This PRN is transmitted back to the earth with a precise time delay. Cross correlation of the transmitted and received signals at the ground station then yields the distance with an accuracy reciprocal to the bandwidth of the PSK. The ranging data is ambiguous modulo the PRN repetition length, which should be kept as short as possible to minimize average transmitter power, i.e., just longer than the distance already known from other measurements. Here, a 1023-bit PRN sequence will be used with a phase-chipping frequency of 60 MHz. This gives a ranging accuracy of 5 m with an ambiguity of 5 km. Instead of returning a single PRN sequence for each one sent up, the transponders may also send multiple ones at lower power. As in GPS receivers, the accuracy is then achieved through signal averaging

5.1.4 Communication

Digital communication between the asteroid and the earth is done by GMSK-PSK on the respective frequencies ν_{dc} and ν_{uc}. The bandwidth is given by the amount of data. In the downlink, the phase slippages ϕ_{ud} between the uplink Doppler carriers and the on-board atomic clock must be transmitted, as well as transponder engineering data. With a stability of 10^{-10} over 1000s, one may expect a maximum phase slippage of 2π radians in 0.2 s for a 15-GHz signal. To transmit this slippage with a resolution of 2π, about 11 to 12 bits of data must be transmitted within 1000 s for each frequency in the coherent link. Leaving a rate of about 100 bits/s for engineering data and error-correction overhead, and assuming a bit-time-bandwidth product of 0.3 for GMSK, a bandwidth of 30 Hz is sufficient for downlink data communication. This is, in fact, of the same order as the scintillation broadening. In order to avoid a power penalty to overcome this broadening, the data can be transmitted in short bursts at, say, 1000-fold bandwidth within time slices of, say, 10 ms once in 10 s. This kind of burst operation is used in cell phones, and requires the same average power as continuous operation. In the uplink, where bandwidth is less critical due to ample available transmitter power, occasional data rates of 100 kbit/s are expected for ground-based computational support of the initial phasing and subsequent refinement, engineering data, software updates, etc.).

5.2 Placement of the Transponders

The transponders are arranged in a web-like structure designed to i) keep them from bouncing off the asteroid and vanish into space, ii) provide communication links between them, iii) distribute electrical power among them, and iv) be deployable under spaceflight conditions.
A sample design fulfilling these requirements is now discussed. It consists of a coarse web spanning over 800 meters (3 times the size of Apophis) with a mesh size of about 100 meters (smaller than Apophis). The wires comprising the web contain carbon fibers for strength, electrical wires, and optical-communication fibers. There are 19 nodes in this web (see fig. 4), each of which spans out a thin Mylar foil, 50 meters in diameter. Distributed over each foil, there are 25 transponder units equipped with multiple antennas, as well as solar cells and electrical and communication links. Each node also carries a compact atomic clock, which can be made to an accuracy of the order of 10^{-10} and weighs only a few grams [34].

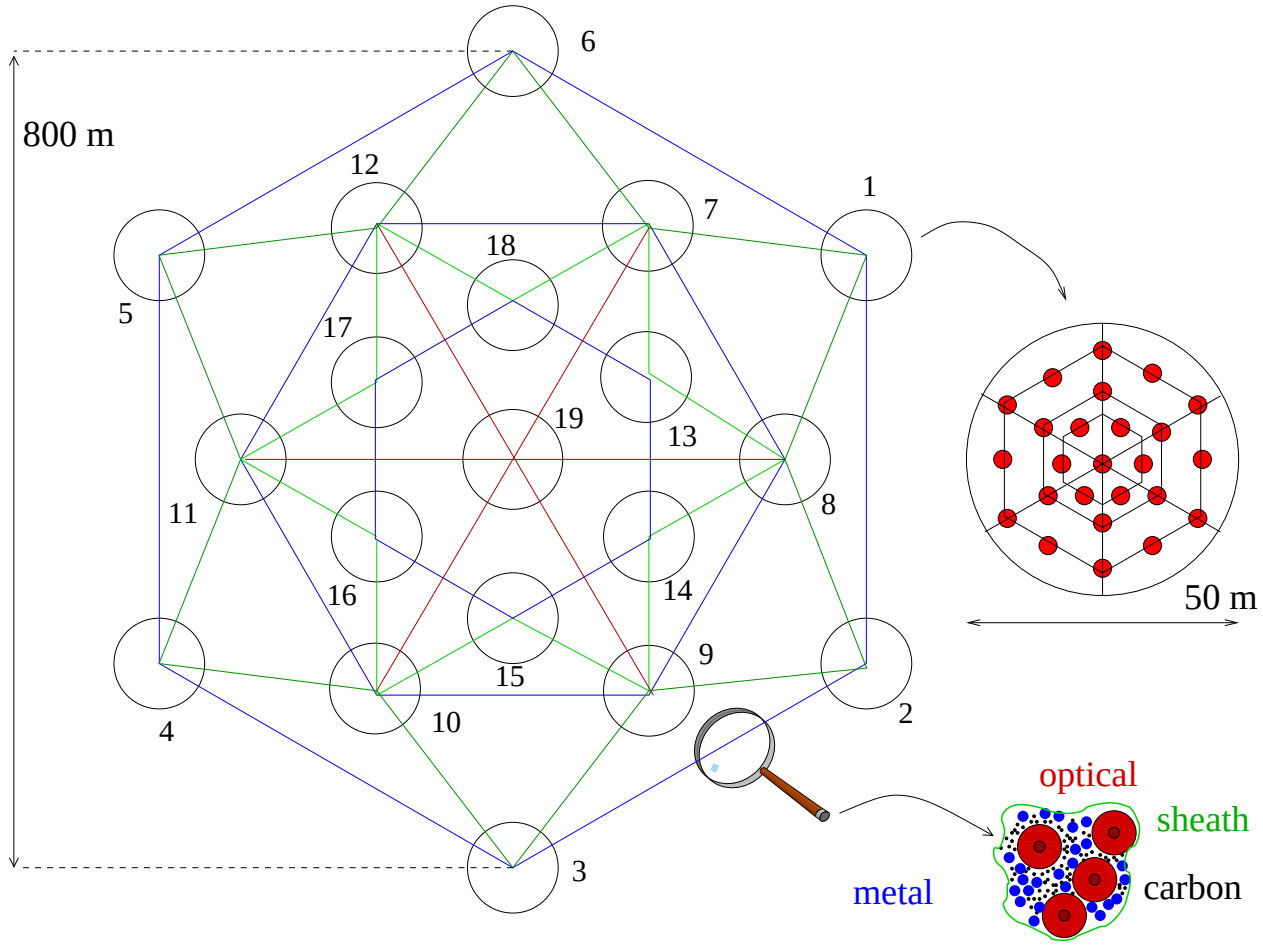

Figure 4: Left: The large web connecting 19 nodes by optical fibers and thin electrical wires. Right: One node containing 25 transponders, connected to each other by optical fibers and thin metal wires attached to a thin Mylar foil. As shown, the total length of wire connecting the nodes is 11.4 km. Lower right: cross section of a wire with carbon fibers, optical fibers, and metal filaments.

5.2.1 The Coarse Web

On the way to the asteroid the web is stowed in a compact configuration inside a transport bus, which, using onboard radar, manouvers to come to a stop about 1 km from the asteroid with a velocity uncertainty of less than 2.5 cm/s (escape velocity at 1 km, eq. (1)). It then deploys the web in a sequence of steps indicated in fig. 5: First, six containers holding the Mylar foils for the

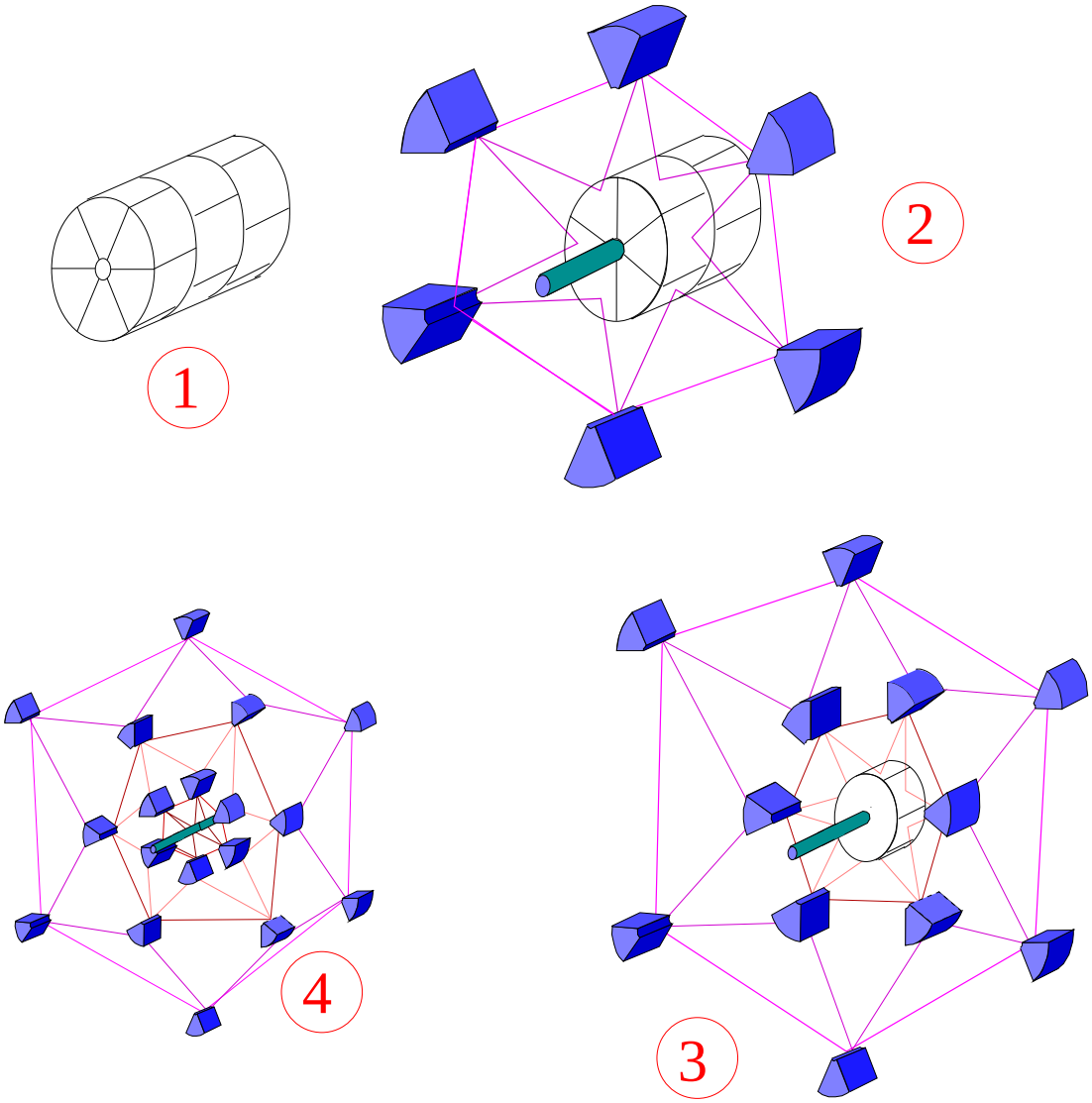

Figure 5: Deployment of the coarse web. A space vehicle (1) carries the array to the asteroid. It is comprised of three sections, each containing six slices. These are ejected in sequence (2-3-4) to deploy the web. After ejection of all slices, the entire web is made to rotate slowly to keep it stretched out (see text). Finally, each of the slices deploys a sub-web, as shown in fig. 6.

outermost nodes (nos. 1 to 6 in fig. 4) are ejected with springs. Shortly thereafter, another set of six containers (7 to 12 in fig. 4) is ejected, and, finally, a third (13 to 18 in fig. 4). As the containers fly

out, they release fine wires that connect them to other ones in the pattern shown in fig. 4. This kind of fiber release is being used for guided missiles and works at much higher velocities than required here. The wires are fine bundles of carbon fibers, 250 metal wires (10μm dia.) and four optical single-mode fibers.

Carbon fibers are being used in space applications, and can be made to tensile strengths of $\sigma = 3000$ MPa to 5000 MPa at a density of about 1.8 g/cm^3 [38]. For a load of 10 N, twice the maximum of 5 N (see pp. 14, 16), discounting the contribution of the optical fibers and metal wires (see below, pg. 14), and conservatively assuming σ =2500 MPa, the carbon-fiber cross section has to be $4 \cdot 10^{-9}$ m^2. Degradation of the mechanical properties under prolonged exposure to space conditions (radiation, etc.) is uncritical because mechanical stresses are negligible after landing.

The metal wires are each 10 microns in diameter, and are made of a high-strength aluminum alloy [39] with a specific resisitivity of $2.9 \cdot 10^{-8}$ Ωm (58% conductivity of the copper standard), and a tensile strength of 100 MPa. Not counting the carbon fibers, the wire assemblies have a resistance of 1.48 Ω per meter. Accounting for some defects, the resistance will be assumed to be 1.5 Ω/m.

The optical fibers provide communication and timing synchronization between the transponders. There are four of them for redundancy, and if all in one wire should break, communication can still be routed indirectly by way of other transponders. The suitability of fibers and other optical-communication components in space applications has been studied extensively [40]. For the purposes of this discussion, a fiber with a total diameter of 125 microns shall be used for an operation wavelength of 1300 nm [40]. It may be interesting to also consider using photonic fibers, which guide the light in air/vacuum in an array of holes at its center, and should thus be less susceptible to attenuation from radiation-induced color centers.

The thermal expansion coefficients differ greatly: $-2 \cdot 10^{-6}$/K... $+ 2 \cdot 10^{-6}$/K for carbon fibers, $0.6 \cdot 10^{-6}$/K for the glass fibers (fused silica), and $24 \cdot 10^{-6}$ for aluminum. To ensure that only the carbon fibers bear mechanical stress, the composite wires should be produced at a lower temperature than anticipated for landing (sec. 5.2.3), and the metal wires should be spun helically around a core of glass and carbon fibers, so they can expand without introducing longitudinal strain. The wires should be coated with a sheath of teflon to prevent fraying in the landing process (sec. 5.2.3).

Now an estimate of the wire mass: With the above cross section and density, the carbon fibers have a specific mass of $8.8 \cdot 10^{-6}$kg/m. The metal wires with a total cross section of $1.96 \cdot 10^{-8}$m^2 and a density of 2700kg/m^3 contribute $53 \cdot 10^{-6}$kg/m, and the four optical fibers with a diameter of 125 μm and a density of 2200kg/m^3 (fused silica) contribute $27.0 \cdot 10^{-6}$kg/m. Finally, with a wire circumference of 750 μm, a 5-micron-thick teflon (2.2 g/cm^3) sheath contributes $8.3 \cdot 10^{-6}$kg/m. This gives a combined specific mass of $89 \cdot 10^{-6}$kg/m, and 12 km (see fig. 4) have a mass of ca. 1070 g.

The fibers and wires have reference marks (colored rings) on them to tell the release mechanisms how much length been released, so that the containers can be stopped gently without rebound. The mechanical stress on the wires due to braking is negligible compared to that in landing (sec. 5.2.3).

Once the coarse web connecting the containers is deployed, small pressurized-gas thrusters on the containers impart a small spin (of the order of 1 rotation per hour) on the web to keep it stretched out. To be able to apply thrusts in the correct directions, the containers have multiple nozzles pointing in different directions.

5.2.2 The Nodes

Once the web is spinning, the folded mylar foils with the transponders are ejected from their containers, and tubes in them (fig. 6) are filled with pressurized gas, making them unfold like an air mattress. Gas pressure is required only until the transponders have settled onto the asteroid surface. To avoid disturbing the array, the containers use their gas boosters used for orienting themselves (sec. 5.2.1) to fly off into space. Attached to the Mylar foil in a pattern shown in fig. 7 are the

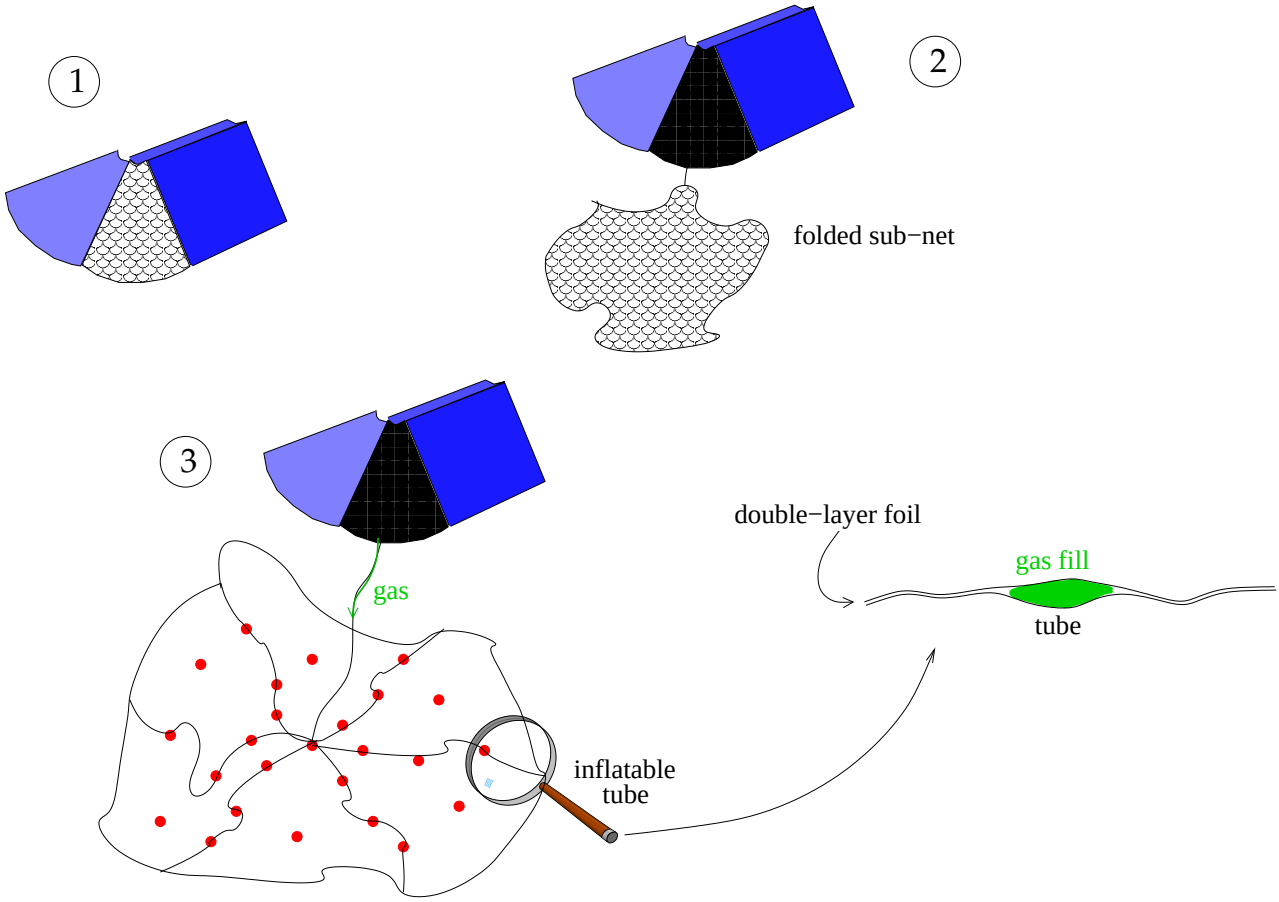

Figure 6: Ejection and unfolding of the sub-webs: 1: container opens, 2: folded Mylar foil is ejected, 3: foil unfolds as gas is blown into tubes formed between two layers of the foil.

transponder units, antennas, optical fibers, electrical wires, and thin-film solar cells.
In addition to the microwave electronics, the central transponder of each node (fig. 7) contains electronics for communication and electric power sharing with other nodes, as well as one compact atomic clock [34].

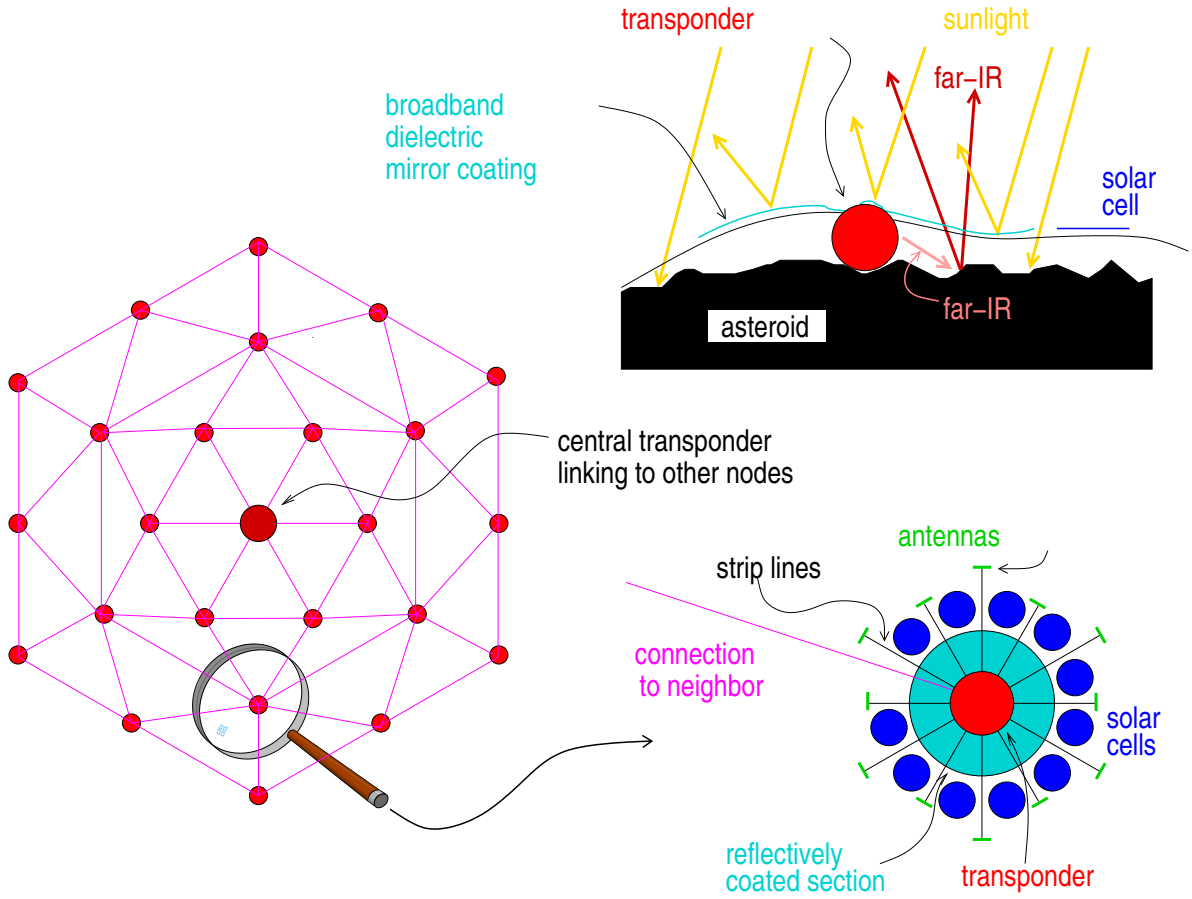

Figure 7: Left: The Mylar foil of one node with the transponders sitting on it. Lower right: Closeup of the foil surrounding one transponder with microwave strip lines going out to the antennas (see sec. 5.6), and a section of Mylar coated with a dielectric-mirror multilayer that reflects visible and near-infrared sunlight, but lets far infrared through (see sec. 5.6). Upper right: Side view of the same. Sunlight is reflected off the coating, but far infrared heat radiation can escape into space. The transponder can thus radiate heat off to the ground surrounding it.

5.2.3 Landing

The fully deployed web has a diameter of 800 m, about three times larger than Apophis. Starting at less than escape velocity from a distance of 1 km, the web slowly falls onto the asteroid, and "impacts" at about 10 cm/s (see sec. 3.2). As its central portion encounters the asteroid, outlying parts continue their motion, are whipped around the asteroid (in slow motion), and get entangled with the other parts of the web (fig. 8).

The kinetic energy in the web is then dissipated over time as the transponders bounce multiple times off the surface of the asteroid while being restrained within the web. Within several hours (sec. 3.2), they come to rest, being held by the weak surface gravity (about 10^{-4} N/kg for Apophis). The bouncing happens in slow motion; even if the kinetic energy of 100 transponders becomes fortuitously concentrated in one, this one would have ten times the original velocity, about 1 m/s.

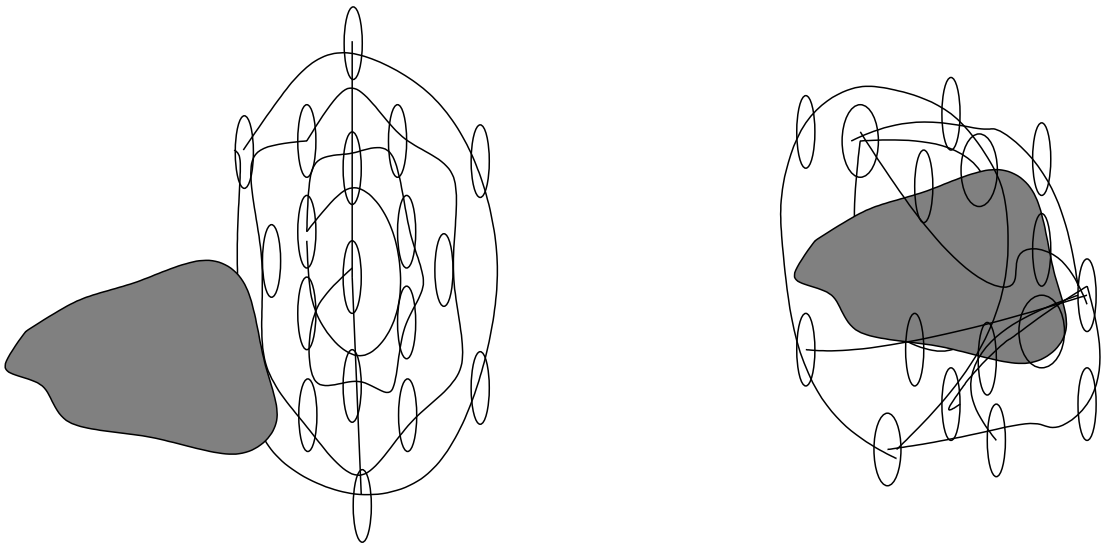

Figure 8: Slow collision of the web with the asteroid, and entaglement.

The maximum stress on the wires of the web occurs during landing, as the nodes pull on them while being slowed down. To prevent fraying due to being dragged across rocky terrain, the wires have a sheath of teflon (see sec. 5.2.1). To limit the stress on the wires, the nodes can release wire with a frictional force of 5 N, just as they do during deployment of the web (sec. 5.2.1). Assume that 10 of the 19 nodes, each with a mass of about 3000 g, and initially moving at 20 cm/s, are brought to a stop by this force; it then takes 1.25 s to stop them, and a wire length of 12.5 cm is realeased in doing so.
As the asteroid rotates, the wires between the nodes experience drastic temperature changes of more than 100 degrees C (comparing to the moon's diurnal temperature variation of up to 250 C). The thermal expansion of the wires of up to $24 \cdot 10^{-6}$/K (sec. 5.2.1)) will then lead to significant length changes (240 mm in a 100-meter-long aluminum wire under a 100-degree temperature change). To prevent the wires from tugging the transponders this way and that with adverse impact on the phasing, the nodes release some extra length of wire after landing.
Photoelectron emission due to solar ultraviolet radiation may charge the asteroid and array, so that electrostatic repulsion overcomes gravity, and the mylar foils with the transponders float off the surface. Although still restrained by the web, they then lose their well-defined phasing. (see electrostatic levitation of dust [41]). If this effect is a problem, then the array can be equipped with a positive-ion emitter similar to the novel ion-drive engines being tested for long-term space missions. The charges are distributed throughout the array by the electrical connections, and the mylar foils can be coated with a weakly conductive layer with Giga-Ohm surface resistivity.

5.3 Transmitter Power

The radiofrequency power P_R received at a distance d from the transmitter is given by the transmitted power P_T, the transmitter antenna gain G_T and the ratio of the effective receiver antenna area A_R

to $4\pi d^2$, i.e., a sphere of radius d. This is conveniently expressed by the Friis formula in terms of the receiver antenna gain $G_R = A_R/\lambda^2$ and the free-space loss $L = (4\pi d/\lambda)^2$

$$P_R = P_T \frac{G_T G_R}{L} \tag{6}$$

Usually, the logarithmic form of this formula is being used, where L is expressed in dB, G_T and G_R are expressed in dBi (gain over an isotropically radiating antenna), and P_T and P_R are expressed in dBm ("m" for milli-Watt).

$$\mathcal{P}_R = \mathcal{P}_T + \mathcal{G}_T + \mathcal{G}_R - \mathcal{L} \tag{7}$$

where $\mathcal{P}_R = (\log_{10} P_R)$[dBm], $\mathcal{P}_T = (\log_{10} P_T)$[dBm], $\mathcal{G}_R = (\log_{10} G_R)$[dBi], $\mathcal{G}_T = (\log_{10} G_T)$[dBi], and $\mathcal{L} = (\log_{10} L)$[dB].

The minimum required transmitter power P_T depends on $\mathcal{G}_T$, $\mathcal{G}_R$, d, and the receiver noise within the signal bandwidth (which may be reduced through autocorrelation techniques, see below). The 70-meter antenna DSN-14 of the deep-space network has a gain of 63.5 dBi at 2.1 GHz, and a G/T (gain over system noise temperature) figure of 51 dBi [42]. In this sample design, each of the 475 transponders has 24 antennas for each radio channel (see sec. 5.6), but only about half of them are in view of the earth at a given time, and random orientations reduce this number by another factor of 1/4 (app. C), so the array effectively consists of 1400 antennas, giving it a gain of 31.5 dBi. The maximum distance d will be assumed to be 1.82 A.U., i.e., $d_{max} = 2.72 \cdot 10^{11}$ m (see sec. 3.1). Then, the free-space loss is $L = 5.7 \cdot 10^{26}$, or $\mathcal{L} = 267.6$ dB at the ranging frequency of ca. 2.1 GHz (tab. 1), about 263 dB for the communication frequency, and 279 dB and 285 dB for the Doppler carriers at 8 and 16 GHz (the dB-sum of the free-space loss and the gain of the ground-based dish antenna is, of course, constant).

For the uplink from ground to the asteroid, a large transmitter power is available, but power consumption of the receivers is an issue. Therefore, it will be assumed that no effort is made to cool the receivers, and only minimal use is made of computationally demanding (i.e., power-consuming) signal processing techniques on the receiver end. The equivalent noise temperature of the receiver antennas and electronics of the transponders will be assumed as 1000 K, which is a typical value for cell phones. This results in a noise spectral density of $1.4 \cdot 10^{-20}$ W / Hz, or -168 dBm/Hz. With the above antenna gains and free-space loss, eq. (7) yields a transmitter power density of 4.6 dBm/Hz (2.9 mW/Hz). With a Doppler carrier frequency of 8 GHz, scintillations during normal solar activity increase the bandwidth to several 10^{-2} Hz (sec. 3.3). Assuming a bandwidth of 0.1 Hz and a noise margin of 20 dB, the transmitter power should then be 14.6 dBm (29 mW) for each frequency used in the multifrequency link (see secs. 5.1.2 and B).

Ranging requires a much higher bandwidth, about 20 MHz for the stipulated accuracy of 5 m and the bandwidth-efficient GMSK modulation scheme with BT=0.3 (see sec. 5.1.3). Scintillations are irrelevant at this bandwidth, so a single frequency is sufficient. The maximum transmitter power of the DSN-14 antenna in the S band (2.1 GHz) is 400 kW (86 dBm) [42]. With the above receiver noise, ranging has then a noise margin of 13 dB, This is less than the 20 dB required for the tolerable bit-error rate of 10^{-3} (sec. 5.1.3). However, as in GPS handsets, the noise margin can be reduced through signal averaging at little expense of computational power.

Finally, the power required for the phasing calibration signal must be calculated with a receiver antenna gain of 0 dBi. With otherwise like parameters, the transmitter power is 36.1 dBm/Hz, that

is 70.9 dBm (12.3 kW) at a bandwidth of 30 Hz (sec. 5.1.1) and 20 dB noise margin.
For the downlink, different conditions apply. The transmitter power is limited, but the receiver can be cooled to reduce the noise, and sophisticated signal-processing procedures can be applied. The system noise temperature of the DSN-14 antenna is about 17 K (deduced from the stated values of 63.5 dBi and 51dBi for gain and G/T [42]). This corresponds to a spectral noise power of -186.3 dBm/Hz, and the transmitter power density is -13.7 dBm/Hz (42μW/Hz). With eq. (7), a bandwidth of 0.1 Hz for the Doppler signal, and a noise margin of 20 dB, the transmitter power should then be -3.7 dBm (420μW). With at least 200 of the 500 transponders in view of the earth at a given time, each of them has then to transmit 2.1 μW per Doppler carrier.
For ranging in the downlink at the maximum distance of 1.82 A.U. with a noise margin of 10 dB, the required transmitter power is 69.3 dBm (8510 W) for a bandwidth of 20 MHz. As above, the lacking 10dB in noise margin need to be obtained through signal averaging. Since this power is shared among at least 200 transponders, each of them needs to output 43 W. There are 24 antennas, each with its own power amplifier, so this is within typical ratings of cell phones: a typical GSM handset transmits bursts of 0.58 ms duration every 4.6 ms at a power of 1 W to 2 W. The bandwidth of 20 MHz required for the ranging accuracy is far larger than that used for in GSM cell phones (25 MHz total, but only 200 kHz for one channel). However, wide-spectrum wireless standards like CDMA come close to this bandwidth [43]. For example, a recent design of an RF power amplifier for operation at 0.9 GHz and 1.9 GHz has more than 10 MHz bandwidth and close to 40% power-added efficiency (PAE) [44].

5.4 Power Requirements, Supply, and Distribution

The calculations in sec. 5.3 show that the Doppler measurement requires very little power (with 20 dB noise margin only 0.08 μW from each transponder for each of the two frequencies). In contrast, ranging requires a peak power of 43 W, but only intermittently. The 1023-bit PRN proposed here takes 16 μs to transmit at a phase-chipping rate of 60 MHz (sec. 5.1.3). Assuming a duty cycle of 10^{-4}, i.e., a transmission rate of 6/s, the average power is a much more manageable 42 mW. For a noise-margin gain of 10 dB, one has to accumulate 100 ranging pulses, so a single ranging measurement takes about 15 s. The central transponder of each node requires an additional 75 mW for the atomic clock [34], and a few mW for fiber-optical communication with the other nodes. Finally, thermal management (mostly cooling) requires considerable power.
In this example, each transponder is assigned a continuous power of 250 mW when in the shade, and 1000 mW when in the sunlight. This accounts for about 100 mW for the onboard digital electronics, microwave receivers, and optical communication, less than 1 mW for the Doppler transmitters even with a power-amplifier efficiency of 20%, 43 mW average for ranging (43 W peak, a conservative estimate (see sec. 5.3) of 10% efficiency for the RF power amplifier, 0.1% duty cycle), and thermal management: 100 mW for heating when in the shade, and ca. 850 mW for cooling when in the sunlight.
The types of power sources that are commonly used in space missions are solar cells and radioisotope thermoelectric generators (RTGs). For reasons given in sec. 4, solar cells seem to be the better choice in the present application. Ample sunlight is available at Apophis' distance from the sun, but the problem of powering the transponders in the asteroid's shadow must be solved. To that end, the

present proposal uses thin, unpaired metal wires to connect the transponders within each node, and also the nodes to each other. Transponders within a node share power through these wires and may send excess power through the node's hub to other nodes, or receive power through the hub from other nodes. To minimize the mass of the long wires between the nodes, a rather high voltage should be used (see below). Within the nodes, the connections are shorter, and the transmission voltage can be lower. Power sharing within a node and among nodes works in similar ways, outlined here only for the latter case:
MOSFET power switches in the hubs of the nodes dynamically connect the wires between the nodes in a sequence of circuit configurations that carry current in loops among them, as shown schematically in fig. 9. At each time, such a current loop contains one or more nodes that drive the current, a number of nodes that consume electric power, and, possibly, some that do not participate in power sharing in a particular configuration within the sequence. The transponders have buffer capacitors that ensure continuous power despite the intermittent, rapidly switched, supply. Because only single wires are used in loops, instead of double-wire point-to-point connections, the high voltages pose no insulation problems. If two wires should touch each other, such as in the crossings shown in fig. 9, they cannot be part of the same current loop. This is not a major problem due to the high redundancy of connections between nodes, but the array will have to perform some tests before deciding upon an optimal configuration of current loops.

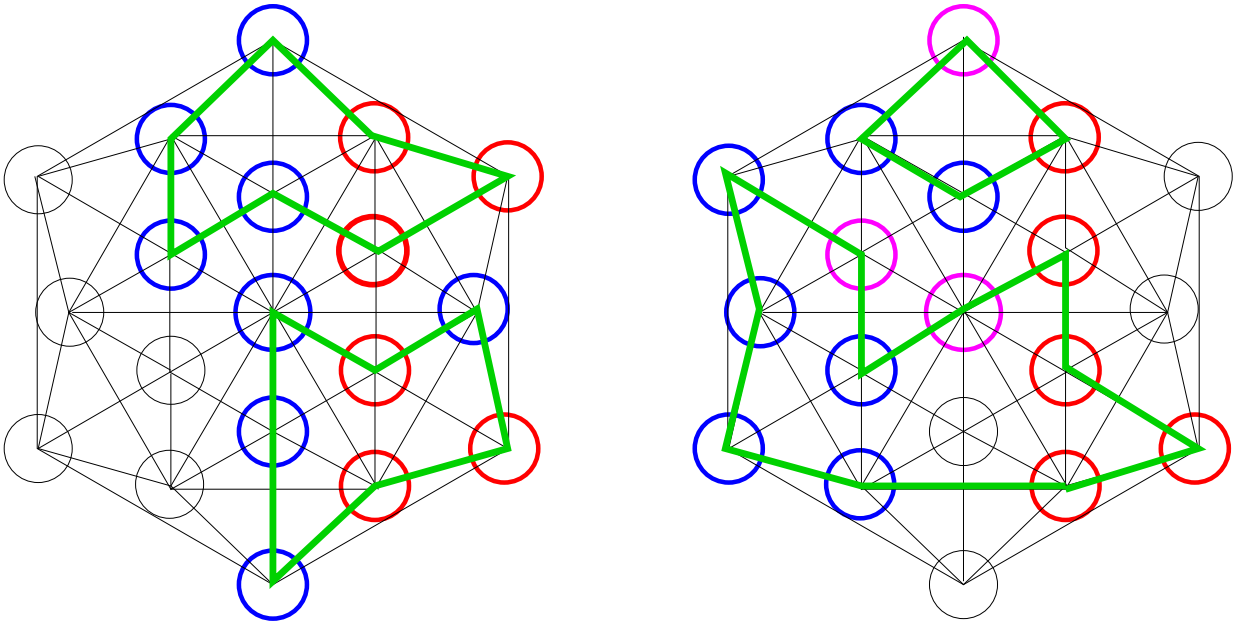

Figure 9: The power-distribution scheme. Current paths are switched rapidly between different configurations, each containing some nodes acting as electric power sources, some as power consumers, and possibly some "spectators". Two possible configurations are shown here with sources in red, consumers in blue, spectators in magenta, and active current paths in green.

Lightweight radiation-tolerant amorphous-silicon solar cells are now available [45]. By depositing the silicon on Kapton foil, a power output of 2 kW per kilogram of solar-cell material can be achieved.

Each transponder will be equipped with 8 W of nominal solar-cell capacity, with a mass of 4 g, each. Accounting for geometry losses due to non-normal incidence of sunlight, the average output is 4 W. Of this power, 1000 mW power the electronics of the transponder itself, 1000 mW are for losses in the power conversion and distribution inside the transponder, and 2000 mW are available for sharing with other transponders within the node and in other nodes. A transponder in the shadow will need at least 350 mW, so that 250 mW are available for use, and 100 mW are conversion losses.
To minimize the weight of the wires connecting the nodes, a high voltage will be used for power transmission: Each of the nodes in a loop (fig. 9) will drive up to 70 mA (time-average) at a voltage up to 700 V (2W from each transponder in the node).
This is now illustrated by example: Suppose there are 10 nodes in a current loop 1.25 km in length (fig. 9), three of which receive sufficient sunlight to power themselves and share 50 W with others (25 transponders in a node, each providing 2 W), one receives sunlight to power only itself, and six nodes are in the shadow. The loop is active τ =50% of the time. With a current of 100 mA in the loop, each of the six power consumers will need a voltage drop of 175 V to draw 8750 mW (25 transponders, 350 mW each, 50%) for a total of 1050 V. The 1.25-km-long wire with 1.5 Ω per meter (sec. 5.2) has a resistance of 1875 Ω, in which the current of 100 mA leads to a voltage drop of 187.5 V. The total voltage drop on the wires and the consumers is thus 1237.5 V, i.e., less than the maximum of 3*700 V that the transponders in the sunlight can provide. The power dissipation of 7.5 mW/m in the wires leads to some minor heating.
The requirement for one node in the sunlight to power two in the shade is conservative because near opposition to earth, when the highest transmitter power is required, most transponders in view of the earth receive full sunlight.

5.5 Phasing of the Array

For all antennas to receive and transmit coherently, phase-stable reference and clock signals must be distributed throughout the array. In the present proposal, each node (see fig. 4) contains a chip-sized atomic clock [34], one of which is determined to be the master. It generates a phase-stable signal at a reference frequency of, say, 84 MHz, a subharmonic of the Doppler frequencies (tab. 1). This frequency is modulated onto a communication laser and transmitted through the fibers, being relayed from one node to the next. Due to the large redundancy of wire connections, it is unlikely that a node, or a transponder within a node, is cut off from this reference. Each transponder then synthesizes locally the carrier frequencies for the signals to be transmitted, as well as for mixing to the received signals for conversion into the baseband (see figs. 11 and 12).
Array phasing for transmission is straightforward; the carriers are synthesized with the appropriate phase shifts, and the PSK modulation of the ranging and communication signals are synchronized by the central clock. These signals then drive the power amplifiers in the transponders.
Reception of signals is more complicated: Within each transponder, the phase-shifted signals from its multiple antennas can be summed directly. However, optical transmission of these radiofrequency sums is not feasible. Instead, each transponder converts its local sum into a lower-frequency baseband, and transmits it for central summing. A similar approach is used in the THousand Element Array radio telescope (THEA) design (see fig. 3.2.1 of ref. [46]).
The web has no central data-processing facility. Signals are distributed to all nodes for processing,

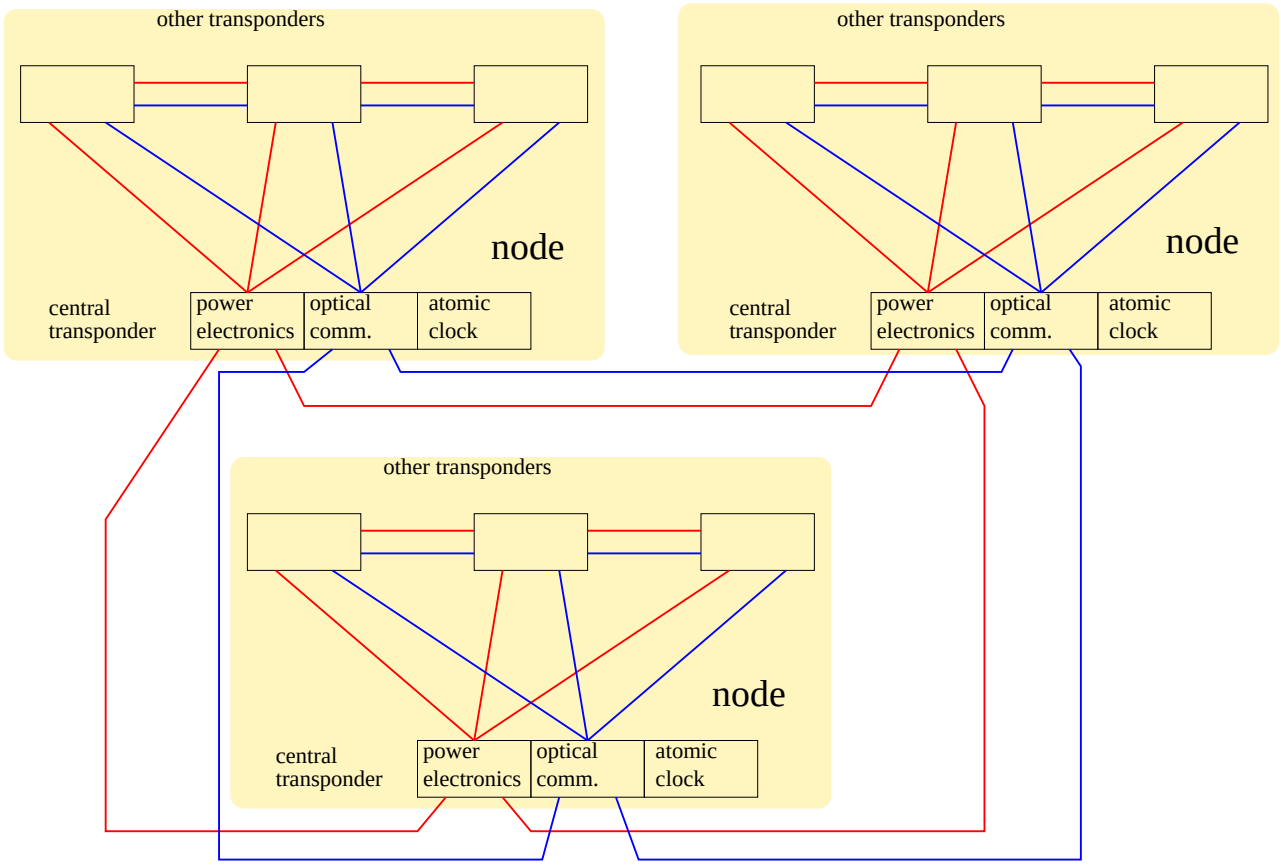

Figure 10: Schematic of the array showing 3 of the 19 nodes, each with the central transponder (see fig. 7) communicating (blue) and sharing power (red) with other transponders of the node, as well as communicating and sharing power with other nodes.

and any node can provide the reference frequency. The nodes check each other for errors, and if one develops problems, it is shut down by "consensus" of the other nodes. This decentralized approach has a high tolerance to component failure.
As the optical fibers change length with the variable sunlight exposure, the reference-frequency signal distributed through them is phase-shifted: in a 200-meter-long fused-silica fiber a temperature change of 100 K leads to a 11-millimeter change in length. This degrades the directionality of the array, and has a severe impact on the phase stability of the Doppler signals. To compensate for this effect, a standard laser-timing technique is used, where the reference signal sent through each fiber is returned through the same fiber, and the phases of the transmitted and returned signals are compared. Because the transponders temperature-controlled, the electronics do not introduce significant sunlight-dependent phase shifts.

5.6 Design of the Transponders

Each of the nodes contains 25 transponders with 120 antennas each, 2*24 for Doppler measurements at 2 frequencies, 24 for communication, 24 for ranging signal reception, and 24 for ranging signal

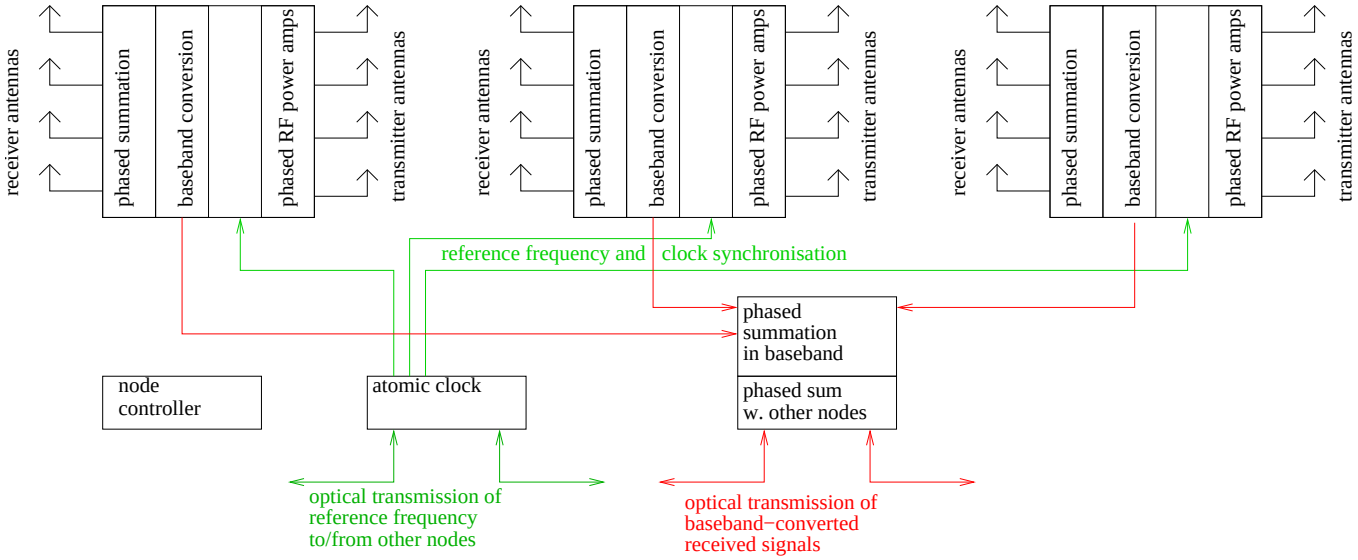

Figure 11: Node electronics showing three of 25 transponders, each with multiple antennas for reception and transmission. The nodes distribute the received and baseband-converted signals across the web for decentralized data processing, and any one node may be providing the reference frequency.

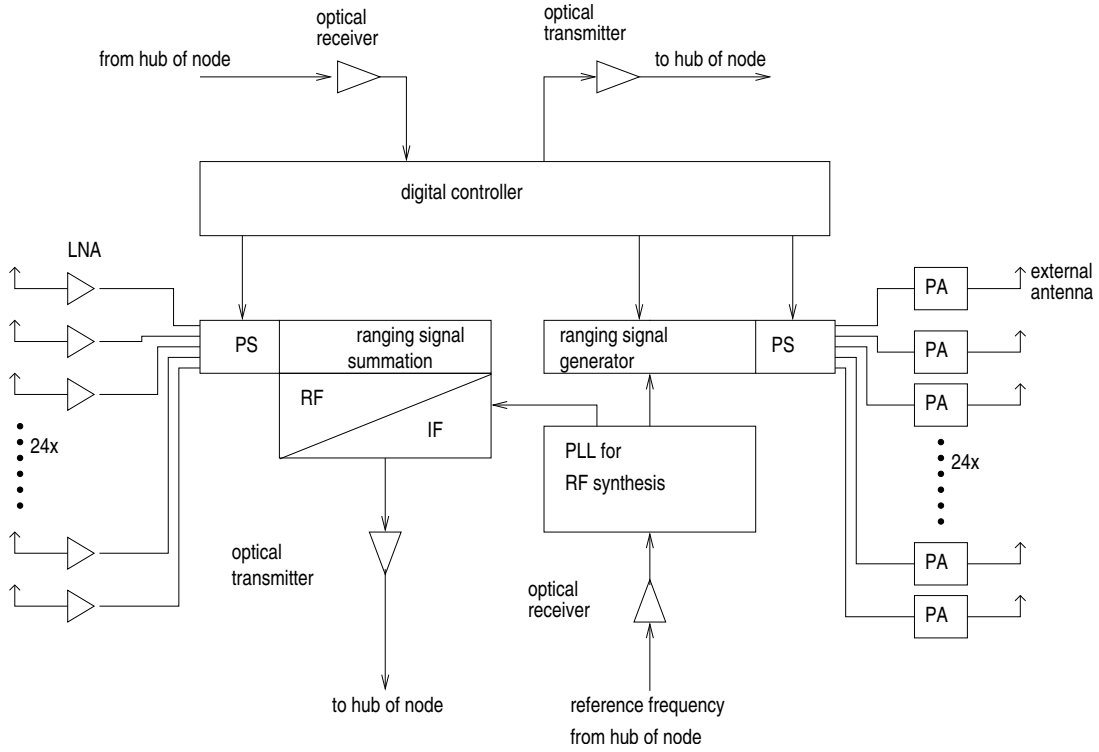

Figure 12: Radiofrequency circuitry for ranging inside each transponder. "PS" means multiple (24x) phase shifters, "LNA" means low-noise amplifier, and "PA" means power amplifier. The Doppler and communications circuits are similar.

transmission. The antennas are printed on the Mylar foil [47], and are arranged around the transponder (see fig. 7). Inside the transponder, a circuit assembly on Kapton foil contains the microwave electronics, digital circuitry, and optical communications circuitry (see fig. 13). There are 24 power

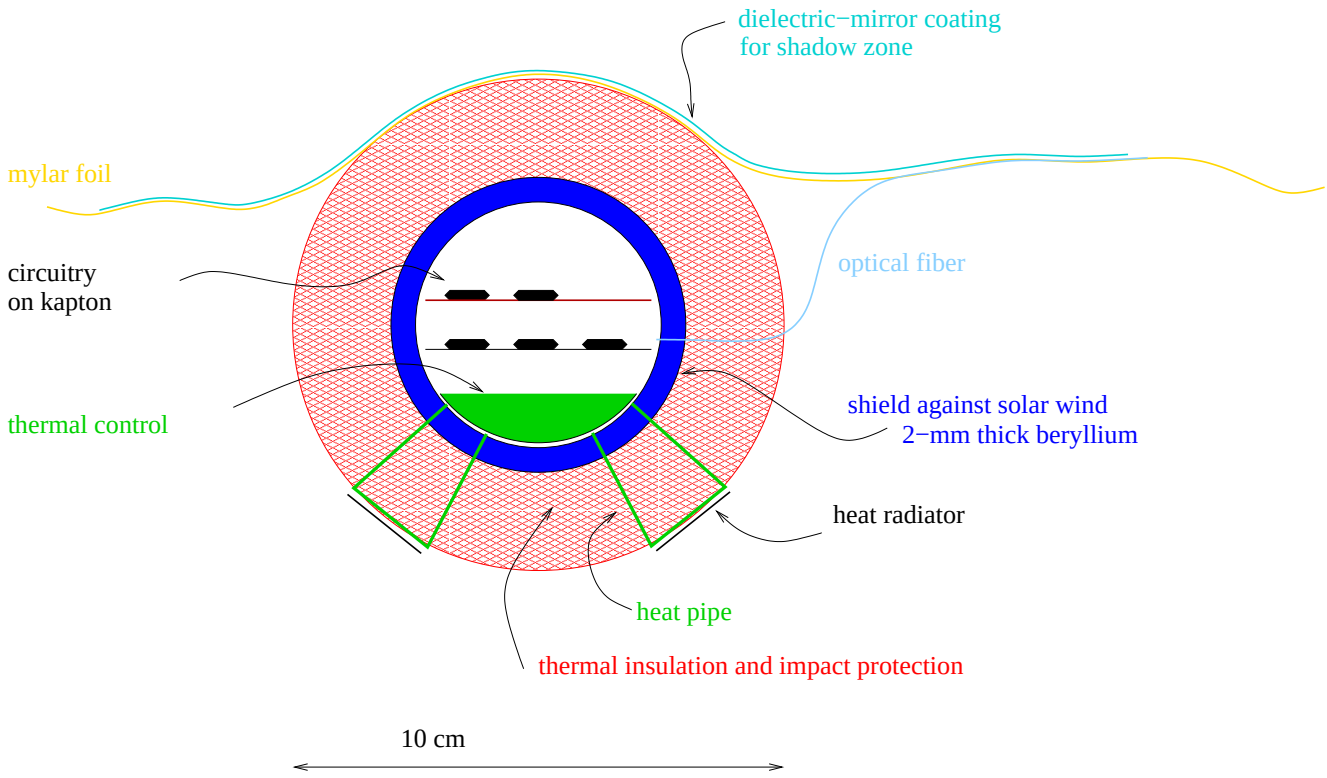

Figure 13: Schematic cut through a transponder, see also fig. 7. The electronics are inside a beryllium shell that protects against lower-energy solar protons (sec. 5.7). A thermal-control unit contains heaters and thermoelectric coolers, and dissipates heat through heat pipes leading to radiators that are in the shadow (see text). The central transponder of each node is slightly larger to hold the electronics for power sharing and communication with the other nodes, as well as the atomic clock.

amplifiers for ranging, two for the two Doppler carriers, and one for communication. The signals are sent to the antennas through digitally controlled phase shifters, as shown in figs. 11 and 12. Likewise, the receivers employ phase shifters.

The electronics are inside a beryllium shell that provides some shielding against protons in the solar wind (sec. 5.7). This shell is filled with a gas for thermal dissipation from the electronics.

The Mylar foil around each transponder has a broadband dielectric coating that reflects visible and near-infrared sunlight but transmits long-wavelength infrared light. This creates shadow zones that are cooled by radiating off heat.[2] The transponders are situated in the shade of this coating, and are thus protected from overheating. The solar cells are, of course on the top side of the Mylar foil.

[2]Far-infrared from the sun gets through, but it comes from a small solid angle compared to 2π for outgoing radiation.

5.7 Radiation Tolerance

The radiation environment of space can disrupt data processing and gradually degrade electronics [48] Commercial electronics used in cell phones are not particularly radiation-tolerant, so special components must be used:

- Microwave components: Radiation-tolerant power amplifiers, mixers, phase shifters, etc., are available for satellite communications from a number of manufacturers, see for example [30] Passive components (resistors, capacitors, etc.) can be assumed to be radiation-tolerant.
- The power-efficient, highly integrated computing technology of cell phones is not radiation-hardened. Equivalent components must be developed using, for example, standard-cell, application-specific integrated-circuitry (ASIC) with a radiation-tolerant process, such as silicon-on-insulator (SOI) CMOS. For faster development times, radiation-tolerant field-programmable logic arrays (FPGA) [49, 50] may also be used. Furthermore, the chip logic and software should include error-detection and correction features.
- Power semiconductors: radiation-hardened power MOSFETs are available, see for example [51]
- Optical-communication equipment, such as lasers, photodetectors, and fibers, have been studied for space applications [40], and radiation-tolerant devices are available.
- lightweight, space-capable solar cells are available [45]
- atomic clocks are found in spacecraft [52], but the compact ones used here [34] must be adapted

The radiation exposure can be reduced by shielding. It is effective against low-energy protons, which comprise most of the solar wind [48]. To limit mass and gain efficiency in dissipating the kinetic energy of the protons, the shielding should consist of light elements like beryllium (see fig. 13).

5.8 Launch Mass

Table 2 shows an overview of the masses comprising the payload. The estimate of the spacecraft mass with fuel tanks and rocket motors is based upon that of the NEAR vehicle [53]. By Tsiolkovsky's equation, the total mass to be delivered to low-earth orbit (LEO) depends exponentially on the total velocity change Δv for rendezvous from LEO. Methods for achieving very low-Δv transits have been developed using many-body dynamics [54], but these typically require very long times. To gain time for mission planning and development, but arrive by early 2014 (see sec. 3.1 and fig. 16), a conventional transit will be chosen here comprised of escape from 200-km LEO ($\Delta v_e = 3.22$ km/s), departure into a transit ellipse (Δv_d), mid-course inclination correction (Δv_i), and velocity matching at arrival (Δv_a). Because Apophis has a small orbit inclination of $\iota = 3.3°$, the problem can be approximated by minimizing $\Delta v_d + \Delta v_a$ in two dimensions, and estimating an upper limit of $\Delta v_i = v_o \tan \iota \approx 1.73$ km/s, where v_o is the orbital velocity of Earth. Such a minimization [55] yields $\Delta v_d + \Delta v_a = 3.76$ km /s for departure on 2012/7/23 and arrival 2013/2/20 (fig. 14). The total is then $\Delta v = \Delta v_e + \Delta v_d + \Delta v_i + \Delta v_a = 7.71$ km/s. Δv is converted to total (payload+fuel) mass using the Tsiolkovsky rocket equation

$$m_t = m_s \exp(\Delta v / v_p), \tag{8}$$

item	unit mass	multiplier	total (g)	comment
transponders	100 g	475	47500	
mylar foil with solar cells, antennas	250 g	19	4750	
atomic clocks w. electronics	25 g	19	475	
power electronics in nodes	100 g	19	1900	
wire between nodes	0.089 g/m	12 km	1070	
containers for the Mylar foil	500 g	19	9500	
other node structures	200 g	19	3800	
spacecraft incl. fuel tanks, rocket engine	80 kg	1	80000	
total			148995	

Table 2: Summary of payload mass.

where m_s and m_t are the payload mass and total mass, and v_p is the rocket exhaust speed. Typical values are $v_p = 4560$ m/s for the space shuttle's hydrogen-oxygen engines [56], and $v_p = 3070$ m/s for the shuttle's hydrazine thrusters [56]. With $v_p = 3070$ m/s, Δv of 7.71 km/s, and a payload of 149 kg (tab. 2), eq. (8) yields 1836 kg. This is a pessimistic estimate because Δv could be reduced by a few 100 m/s with a moon flyby, Δv_i is an upper estimate, and LEO breakout could follow right after LEO insertion, so hydrogen/oxygen engines with $v_p = 4560$ m/s could be used for Δv_e.

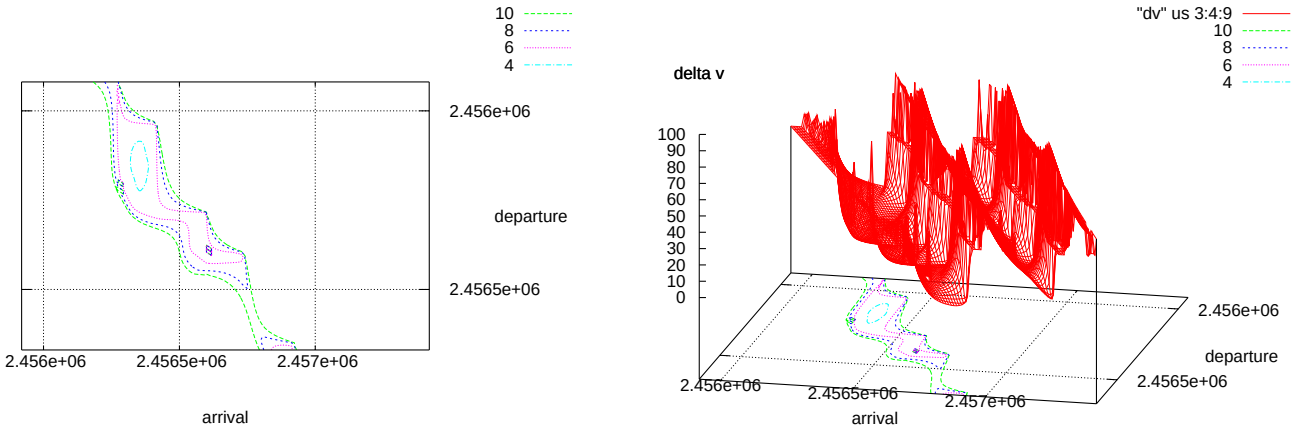

Figure 14: Arrival vs. departure dates for total velocity changes $\Delta v_d + \Delta v_a = 4$, 6, 8, 10 km/s for departure from earth after LEO breakout, and rendezvous with Apophis. Minimum Δv for departure on epoch 2456132 (2012/7/23), arrival on epoch 2456345 (2013/2/20), see fig. 16. Program available at [55], similar plots in ref. [57].

5.9 Cost Estimate

This project requires funding for the design of the transponders and related equipment, for testing, for launching, and for operation (staff and antenna time). Table 3 gives an overview of the estimated costs, based upon a gross salary (including benefits and overhead) of $250000 for one engineering man-year. The launch cost is based on $20000 per kg [58, 59]. Antenna time is assumed to be free through the scientific proposal system. The estimate includes four launches of subsystems to test performance under space conditions. This kind of test may be necessary for the unfolding of the web, and could share a ride with a commercial satellite.

item	man-years	time (yr)	cost (k$)	comment
transponders, electrical design	10	1	2500	labor
transponders, mechanical design	1		250	labor
web, design of unfolding mechanism	15	1	3750	labor
RF test and meas. equipment			1000	scopes, netw. anal., etc.
vacuum, radiation test equipment			1500	
final assembly	1	0.5	350	parts and labor
launch of 1836 kg into LEO			36720	
launch 50 kg to LEO		4	1000	component tests
operation for 5 years	10	5	2500	
total			49570	

Table 3: Cost estimate.

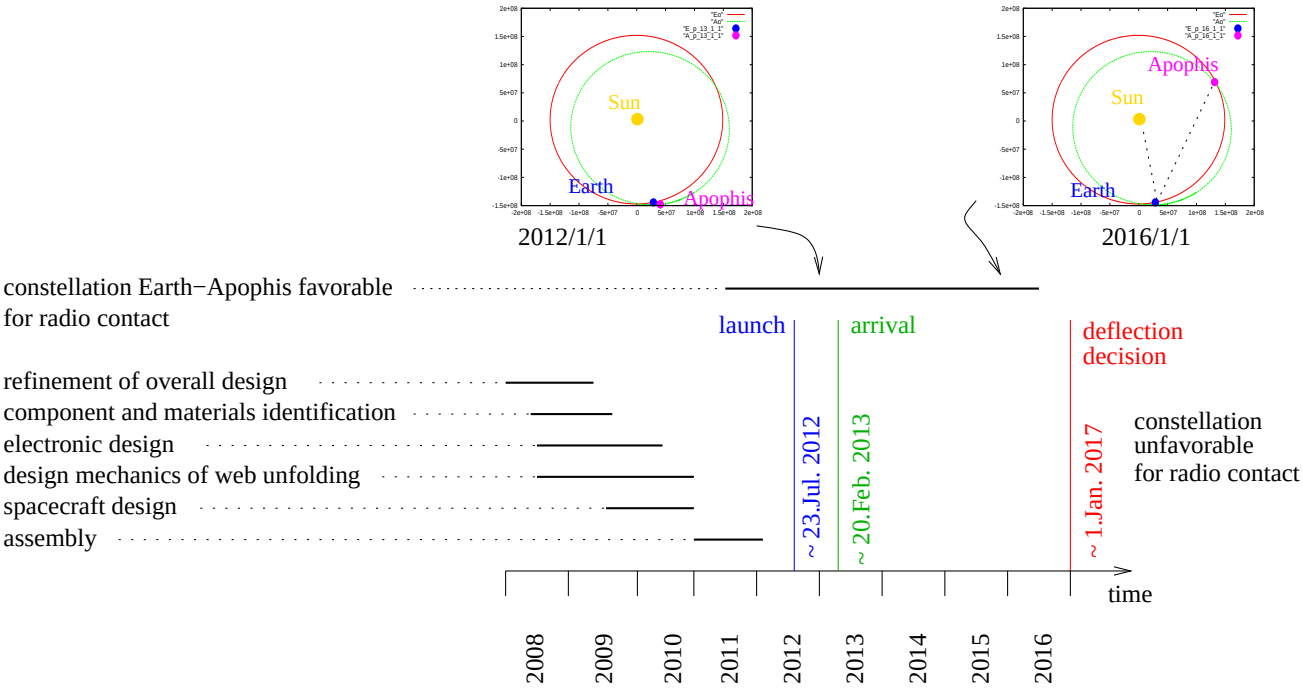

Figure 15: Project timeline

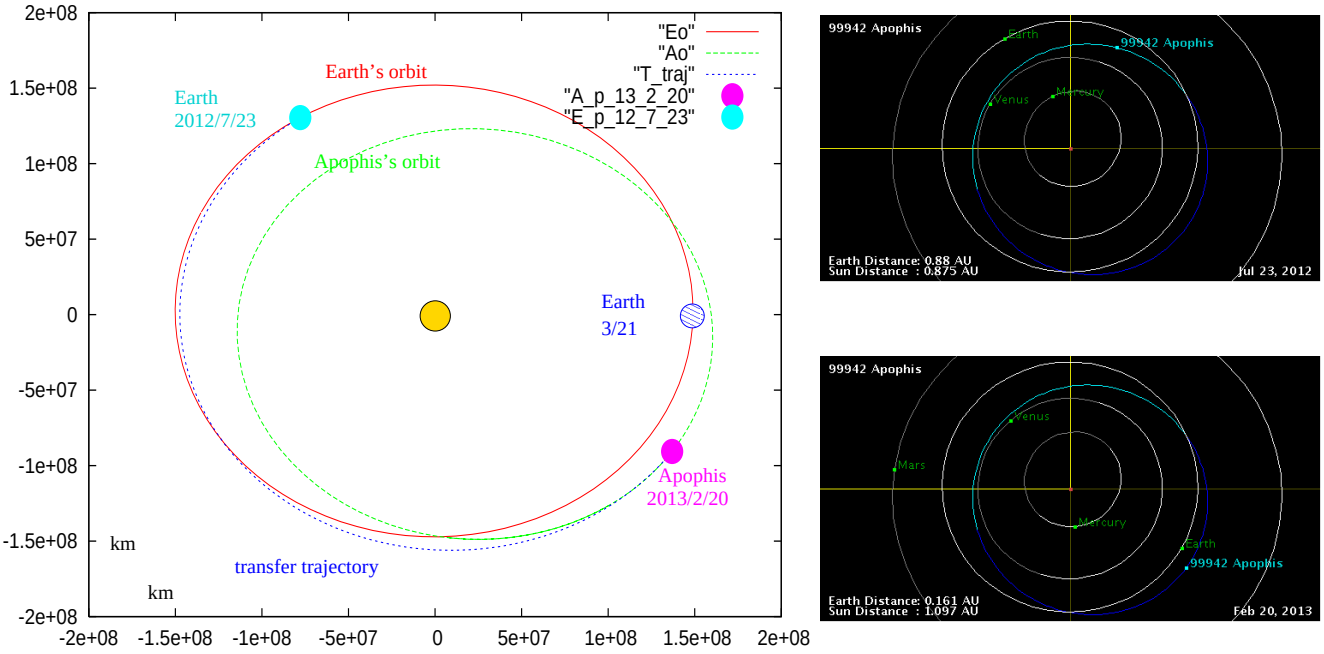

Figure 16: Left: Launch ca. 23. Jul. 2012, arrival ca. 20. Feb. 2013 [55], Right: corresponding graphs from JPL [60].

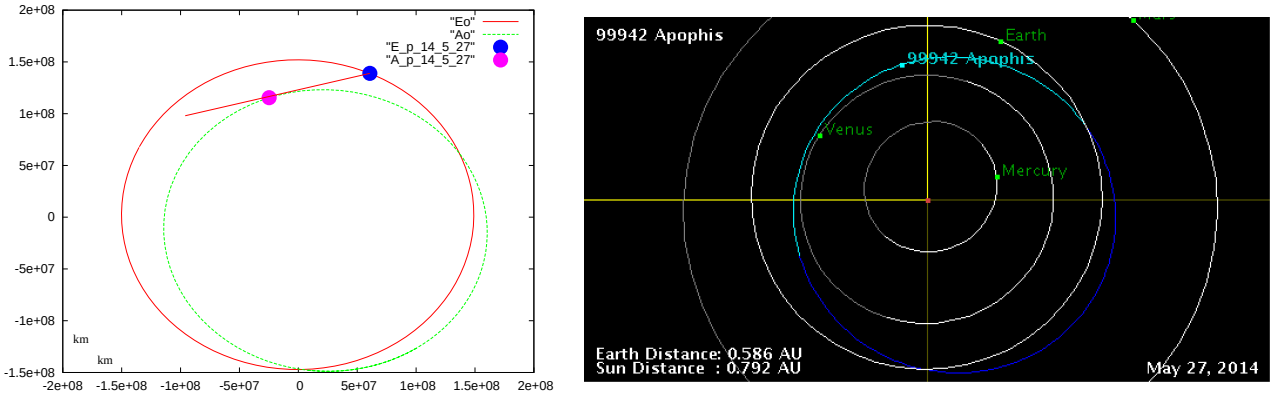

Figure 17: Tangential line-of-sight [55, 60]

Acknowledgments

Freely available technical literature was essential to the development of this proposal. Important sources were the Smithsonian/NASA server at http://adswww.harvard.edu/, the b612 foundation at http://www.b612.org, and, of course, google. I would also like to thank Dr. Dieter Teuber for his valuable comments on radiation tolerance of electronics.

Appendix

A Doppler Shift from Phase Slippages

A frequency ν_{ud} sent from the ground to the asteroid is received there as $\nu_{ud}^{(d)} = \nu_{ud}(1 - v_r/c)$, where v_r is the radial velocity of the asteroid relative to the earth ($v_r > 0$ if the mutual distance increases with time). Comparison with a clock on the asteroid running at a frequency of $\nu_{ud}^{(i)}$ gives a beat frequency $\Delta\nu_{ud} = \nu_{ud}^{(d)} - \nu_{ud}^{(i)}$

$$\Delta\nu_{ud} = \nu_{ud}\left(1 - \frac{v_r}{c}\right) - \nu_{ud}^{(i)} \tag{9}$$

Likewise, a frequency ν_{dd} sent from the asteroid is received on the ground as $\nu_{dd}^{(d)} = \nu_{dd}(1 - v_r/c)$. Being derived from the same clock, $\nu_{ud}^{(i)}$ and ν_{dd} are coherent, i.e., $\nu_{ud}^{(i)} = \alpha\nu_{dd}$ with a constant factor α. Comparison with a frequency $\nu_{dd}^{(i)}$ derived from the ground-based clock gives the beat frequency

$$\Delta\nu_{dd} = \nu_{dd}\left(1 - \frac{v_r}{c}\right) - \nu_{dd}^{(i)} \tag{10}$$

The frequencies $\nu_{dd}^{(i)}$ and ν_{ud} are derived from the same ground-based clock, so $\nu_{dd}^{(i)} = \beta\nu_{ud}$.
The beat frequency $\Delta\nu_{ud}$ is transmitted through the digital channel, so both $\Delta\nu_{dd}$ and $\Delta\nu_{ud}$ are known on the ground. Substituting $\nu_{dd}^{(i)} = \beta\nu_{ud}$ in eq. (10) yields

$$\nu_{dd} = \frac{\Delta\nu_{dd} + \beta\nu_{ud}}{\left(1 - \frac{v_r}{c}\right)} \tag{11}$$

Substituting this into eq. (9), and using $\nu_{ud}^{(i)} = \alpha\nu_{dd}$ yields then

$$\Delta\nu_{ud} = \nu_{ud}\left(1 - \frac{v_r}{c}\right) - \alpha\frac{\Delta\nu_{dd} + \beta\nu_{ud}}{\left(1 - \frac{v_r}{c}\right)}, \tag{12}$$

that is, a quadratic equation for $(1 - v_r/c)$

$$0 = \nu_{ud}\left(1 - \frac{v_r}{c}\right)^2 - \Delta\nu_{ud}\left(1 - \frac{v_r}{c}\right) - \alpha\Delta\nu_{dd} + \alpha\beta\nu_{ud}, \tag{13}$$

B Multifrequency Doppler Measurements

As the gravitational-wave experiment on the Cassini spacecraft has demonstrated, radio Doppler measurements accurate to about 1 micron per second are possible in space [33]. To eliminate the effect of plasma scintillations, this experiment has to use two frequencies (see sec. 5.1.2). In the present application, the requirements are somewhat different, and one frequency would be sufficient, in principle (see below). Nonetheless, there are advantages to using two frequencies (also below).
Insertion-and-removal of a refractive medium, such as the interplanetary plasma has no net effect on the phase of a radio signal. As long as the refractive index of this medium is bounded ($< \infty$),

the spectral broadening of a monochromatic radio signal asymptotically goes to zero with increasing integration times. Therefore, a single frequency is sufficient if very long integration times are feasible. In a gravitational-wave (GW) experiment one is interested in a large bandwidth of the GW (here mHz, as opposed to μHz), which is reciprocal to the integration time τ of the radio signal. To keep the integration times as short as possible, the effect of scintillations must be eliminated by use of at least two radio frequencies and the dispersion relationship of the refractive index, eq. (3). Even so, a radio signal of 10^{10} Hz must be measured for 1000 s to count off 10^{13} oscillations, and thus reach an accuracy of 10^{-15} at a phase accuracy of $2\pi/100$ radians (a realistic value for microwave technology). In the case of the asteroid, the prinipal bandwidth limitation is reciprocal to a fraction of the orbital period, i.e., days to months. Therefore, a single frequency could be used for Doppler measurements. There are, however, practical limitations, such as available time on the ground-based antennas, and the lengths of time intervals without any disturbance (weather, etc.). Furthermore, a second Doppler frequency adds minimally to the mission complexity, requiring only a small amount of electric power in the transponders (see sec. 5.4), some additional antennas on each transponder, and some additional microwave circuitry. Thus, the two-frequency Doppler technique appears to be the best choice.

C Random Phased Array

Consider an array of N randomly oriented dipoles fed with a total power P distributed evenly among them. The amplitude radiated from each dipole in a given direction and a given polarization is proportional to the projection of the dipole vector onto the polarization vector (fig. 18). The power $\mathcal{P}$ received is proportional to the square of the sum over all amplitudes:

$$\mathcal{P} \sim \left(\sum_i \sqrt{\frac{P}{N}} \cos\Theta_i \right)^2 \tag{14}$$

where Θ is the angle between the dipole and the polarization. For many dipoles the sum may be replaced with an integral, where each dipole is represented by an area of $2\pi/N$ on the upper half of the unit sphere (fig. 18):

$$\mathcal{P} \sim \left(\sqrt{\frac{P}{N}} \frac{N}{2\pi} \int_0^{\pi/2} \cos\Theta \int_0^{2\pi} \sin\Theta d\phi d\Theta \right)^2 = \frac{PN}{4} \tag{15}$$

The integral $\cos\Theta \sin\Theta$ between the limits $0 \ldots \pi/2$ gives $1/2$, so the gain of this random array is $N/4$ (assuming proper phasing of the antennas for the direction towards the receiver).

D Science/Other Applications

Besides the immediate purpose of measuring the orbit of Apophis, the mission can provide data on its physical properties that will help to better prepare a deflection mission of this or other asteroids. Most of all, the surface composition should be determined, so that a deflection device can be attached. Other helpful science data would be on the Yarkovski effect. Furthermore, science applications

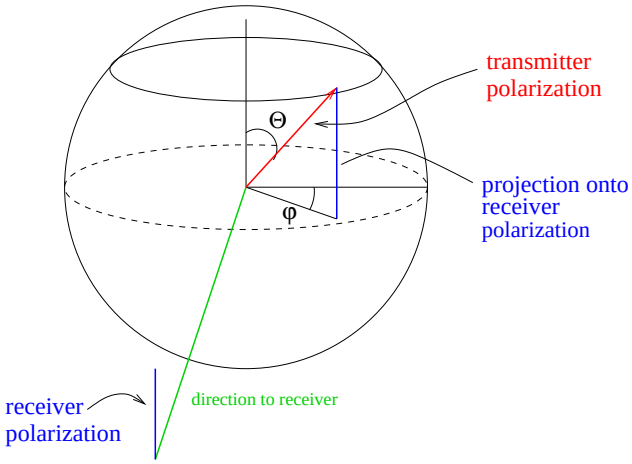

Figure 18: Sphere representing uniform distribution of random dipole orientations.

unrelated to threat mitigation would be interesting in their own right, and could be used to attract funding that indirectly benefits the threat mitigation. Finally, a mission to Apophis can be seen as a first test run for a commercial exploitation of asteroids [27].

Within the present proposal, a determination of the surface composition can be done in complementary ways: For one, some of the transponders could be equipped with small cameras similar to those integrated into cell phones. The launch mass penalty due to these cameras would be negligible, and the image data could be transmitted through the digital communication channel (sec. 5.1.4). Complementary to these 'ground-based" observation, a high-resolution imager may also be installed on the carrier vehicle, which may be left in orbit around the asteroid after ejection of the web.

The image data thus obtained will be very useful for planning a deflection mission: If the asteroid has the composition of a pile of rubble, then the kinetic-impact option may be not very useful. Information on the surface composition will also be important in finding ways of attaching a deflection device (rocket, etc.). If the surface consists of loose gravel, it may be possible to land a device that digs up gravel, and ejects it with a solar-powered catapult. This would eliminate the need to carry large amounts of fuel for a deflection rocket.

A better understanding of the Yarkovski effect would help in the precise orbit determination of this and other asteroids, so that long-term threat prediction can be made. The array provides information on the asteroid's acceleration through precise velocity measurement, and on changes in the rotation rate (Yarkovski-O'Keefe-Radzievskii-Paddack effect) through logging of the array phasing to track the direction towards the earth. In the same way, the alteration of the asteroid's rotation due to tidal forces during the close passage in 2029 [61] can be measured.

An interesting science application of the array would be to use it as a radio telescope, and link it to earth-based ones into a very-long-baseline interferometer (VLBI). VLBI realized to date has baselines up to the diameter of the earth. Having an additional radio telescope at distances up to about 1.82 AU would greatly improve the resolution (within limits given by scintillations). Because this distance varies with the asteroid's orbit, a large range of spatial Fourier components of a given object can be measured over time.

Another interesting science application would be the search for long-wavelength gravitational waves, similar to the experiment on the Cassini spacecraft [16].

E In-situ Linking of Independently Launched Arrays

To further increase the tolerance for component failure, multiple webs with transponders might be independently launched and landed on the asteroid. They could then combine into one large array through short-range radio links for the synchronization of reference frequencies and digital communication. For two webs to combine into one, it is sufficient to have any one transponder in one web to establish communication with any one transponder in the other one. A concern would be, however, the increased probability of electric wires crossing each other, thus restricting the possible power-sharing circuit configurations (see sec. 5.4).

F Possible Funding from Cell-Phone Manufacturers

The choice of frequencies, modulation, communication protocols, etc., allows the claim that the transponders are based upon cell-phone technology, even if some major adaptations to the space environment are necessary (radiation hardening, etc.). It may thus be possible to win a major cell-phone manufacturer to sponsor the orbital-tracking mission.

References

[1] JAXA. Itokawa. *web document*, 2007. `http://www.isas.jaxa.jp/e/snews/2005/1102.shtml`.

[2] NASA. Earth fact sheet. *web document*, 2007. `http://nssdc.gsfc.nasa.gov/planetary/factsheet/earthfact.html`.

[3] S.J. Ostro. Radar observations of earth-approaching asteroids. *Engineering and Science*, 60:24–31, 1997. `echo.jpl.nasa.gov/~ostro/ostro_es_1.5meg.pdf`.

[4] G.B. Valsecchi, A. Milani, G.F. Gronchi, and S.R. Chesley. Resonant returns to close approaches: Analytical theory. *Astronomy and Astrophysics*, 408:1179–1196, 2003. `copernico.dm.unipi.it/simca/preprints/2002/June02/valsecchi_1.ps.gz`.

[5] S.R. Chesley. Potential impact detection for near-earth asteroids: the case of 99942 apophis (2004 mn4). *Asteroids, Comets, Meteors Symp.*, s22:215–228, 2005. `http://journals.cambridge.org/action/displayAbstract;jsessionid=0F7877259F7844279C012F3E669AEC5A.tomcat1?fromPage=online&aid=414764`.

[6] NASA. Near earth object program. *web document*, 2007. `http://neo.jpl.nasa.gov/risk/a99942.html`.

[7] P.W. Chodas and D.K. Yeomans. Predicting close approaches and estimating impact probabilities for near-earth objects. *AAS Astrodyn. Specialist Conf. paper 99-462*, 111:1–4, 1999. `http://trs-new.jpl.nasa.gov/dspace/handle/2014/18049`.

[8] R. Schweickart, C. Chapman, D. Durda, P. Hut, B. Bottke, and D. Nesvorny. Threat Characterization: Trajectory Dynamics. *White paper no. 39 at NASA NEO Workshop held in Vail, Colorado, 26-28 June, 2006*, 2006. www.b612foundation.org/papers/wpdynamics.pdf.

[9] R. Schweickart, C. Chapman, P. Hut, and D. Durda. Threat Mitigation: The Asteroid Tugboat. *White paper no. 41 at NASA NEO Workshop held in Vail, Colorado, 26-28 June, 2006*, 2006. arxiv.org/pdf/physics/0608156.

[10] B612 Foundation. *web site*, 2007. http://www.b612foundation.org.

[11] R. Schweickart, C. Chapman, P. Hut, and D. Durda. Threat Mitigation: The Gravity Tractor. *White paper no. 42 at NASA NEO Workshop held in Vail, Colorado, 26-28 June, 2006*, 2006. www.b612foundation.org/papers/wpGT.pdf.

[12] D. Vokrouhlicky. Diurnal Yarkovsky effect as a source of mobility of meter-sized asteroidal fragments. I. Linear theory. *Astronomy and Astrophysics*, 335:1093–1100, 1998. http://astro.mff.cuni.cz/davok/papers/v98_aaI.pdf.

[13] D.K. Yeomans, P.W. Chodas, M.S. Keesey, S.J. Ostro, J.F. Chandler, and I.I. Shapiro. Asteroid and comet orbits using radar data. *Astron. J.*, 103:303–317, 1992. http://adsabs.harvard.edu/abs/1992AJ....103..303Y.

[14] S.J. Ostro. Radar contributions to asteroid astrometry and dynamics. *Cel. Mech. Dyn. Astron.*, 66:87–96, 1996. http://adsabs.harvard.edu/abs/1997CeMDA..66...87O.

[15] R. Woo, F.-C. Yang, K.W. Yip, and W.B. Kendall. Measurements of large-scale density fluctuations in the solar wind using dual-frequency phase scintillations. *Astrophys. J.*, 210:568–574, 1976. http://adsabs.harvard.edu/abs/1976ApJ...210..568W.

[16] S.W. Asmar, J.W. Armstrong, L. Iess, and P. Tortora. Spacecraft Doppler tracking: Noise budget and accuracy achievable in precision radio science observations. *Radio Science*, 40:1–9, 2005.

[17] G. Lantoine. Optimal trajectories for soft landings on ateroids. *AE8900 MS Special Problems Report, Space Systems Design Lab, Ga Tech*, 2006. http://www.ssdl.gatech.edu/Papers/Masters/Special\%20Problem\%20Report_Lantoine.pdf.

[18] A. Rossi, F. Marzari, and P. Farinella. Orbital evolution around irregular bodies. *Earth Planets Space*, 51:1173–1180, 1999. http://www.terrapub.co.jp/journals/EPS/pdf/5111/51111173.pdf.

[19] J.W. Armstrong. Low-frequency gravitational wave searches using spacecraft Doppler tracking. *Living Review Relativity*, 9:1–56, 2006. http://relativity.livingreviews.org/Articles/lrr-2006-1/.

[20] J.W. Armstrong and R.A. Sramek. Observations of tropospheric phase scintillations at 5 ghz on vertical paths. *Radio Science*, 17:1579–1586, 1982.

[21] J.D. Jackson. *Classical Electrodynamics, 2nd ed.* John Wiley and Sons, New York, 1975.

[22] R. Woo, F.-C. Yang, and A Ishimaru. Structure of density fluctuations near the sun deduced from pioneer-6 spectral broadening measurements. *Astrophys. J.*, 210:593–602, 1976. http://adsabs.harvard.edu/abs/1976ApJ...210..593W.

[23] D.D. Morabito. Solar corona-induced fluctuations on spacecraft signal amplitude observed during solar superior conjunctions of the Cassini spacecraft. *Radio Science*, 42:003425, 2007.

[24] W.M. Cronyn. The analysis of radio scattering and space-probe observations of small-scale structure in the interplanetary medium. *Astrophys. J.*, 161:755–763, 1970. http://adsabs.harvard.edu/abs/1970ApJ...161..755C.

[25] W.M. Cronyn. Density fluctuations in the interplanetary plasma: Agreement between spaceprobe and radio scattering observations. *Astrophys. J.*, 171:L101–L105, 1972. http://adsabs.harvard.edu/abs/1972ApJ...171L.101C.

[26] R. Woo. Radial dependence of solar wind properties deduced from helios 1/2 and pioneer 10/11 radio scattering observations. *Astrophys. J.*, 219:727–739, 1978. http://adsabs.harvard.edu/abs/1978ApJ...219..727W.

[27] M. Sonter. Near earth objects as resources for space industrialization. *Solar System Development Journal*, 1:1–31, 2001. phoenix8.physics.miami.edu/resonance/ssdj(2001)1(1)1-31msonter.pdf.

[28] ESA. esa Rosetta. *web document*, 2007. http://www.esa.int/SPECIALS/Rosetta/ESAMXF7708D_0.html.

[29] M.A. Ingram, R. Romanofsky, R.Q. Lee, F. Miranda, Z. Popovic, J. Langley, W.C. Barott, M.U. Ahmed, and D. Mandl. Optimizing satellite communications with adaptive and phased array antennas. *Proc. 2004 Earth Science Technology Conference, Palo Alto, CA, June 22-24, 2004*. http://eo1.gsfc.nasa.gov/new/validationReport/Technology/SensorWebs/EO-1%20Optimizing%20Satellite%20Communications.pdf.

[30] Mimix broadband. *web site*, 2007. http://www.mimixbroadband.com/satellite.asp.

[31] United states frequency allocations. *web document*, 2007. http://www.ntia.doc.gov/osmhome/allochrt.pdf.

[32] Deutsches Zentrum für Luft-und Raumfahrt. 99942 apophis. *web document*, 2007. http://earn.dlr.de/nea/099942.htm.

[33] P. Tortora, L. Iess, J.J. Bordi, J.E. Ekelund, and D.C. Roth. Precise Cassini navigation during solar conjunctions through multifrequency plasma Calibrations. *J. of Guid., Control, and Dyn.*, 27:251–257, 2004. http://www.aiaa.org/content.cfm?pageid=406&gTable=japaper&gID=997.

[34] National Institute of Standards and Technology. Chip-scale atomic devices at nist. *web site*, 2007. http://tf.nist.gov/ofm/smallclock/index.htm.

[35] Agilent Technologies. GSM design library. *web document*, 2005. http://eesof.tm.agilent.com/docs/adsdoc2005A/gsm/gm013.html.

[36] Plextek Ltd. Introduction to digital modulation schemes. *web document*, 2007. http://www.plextek.com/papers/schmsv6.pdf.

[37] European Standard. Gsm 05.05 v8.5.1. *web document*, 1999. http://ham.zmailer.org/oh2mqk/GSM/GSM-05.05.pdf.

[38] Hexcel.com. Carbon fibers. *web site*, 2007. http://www.hexcel.com/Products/Carbon+Fibers.

[39] T. Horikoshi, H. Kuroda, M. Shimizu, and S. Aoyama. Development of aluminum alloy conductor with high electrical conductivity and controlled tensile strength and elongation. *Hitachi Cable*, 2006. http://www.hitachi-cable.co.jp/ICSFiles/afieldfile/2006/10/16/h_06.pdf.

[40] K.A. LaBel, C.J. Marshall, P.W. Marshall, P.J. Luers, R.A. Reed, M.N. Ott, C.M. Seidleck, and D.J. Andrucyk. On the suitability of fiber optic data links in the space radiation environment: a historical and scaling technology perspective. *Proc. Aerospace Conf.*, 1998:421–434, 1998. nepp.nasa.gov/photonics/pdf/ieeeaero.pdf.

[41] T.E. Bell. Moon fountains. *web article*, 2005. http://science.nasa.gov/headlines/y2005/30mar_moonfountains.htm.

[42] R. Miller. Deep space network status. *web document*, 2006. www.ioag.org/ioag6_nasajpl_dsn_status.pdf.

[43] W.K.M. Ahmed and E. Kpodzo. Interface considerations for SDR using digital transmitters. *RF Design*, 5:10–19, 2005. http://rfdesign.com/mag/radio_interface_considerations_sdr/.

[44] W. Ahmed, D. Bengtson, and P. O'Horo. DTx: a revolutionary digital transmitter technology to providemulti-mode/multi-band Capability. *SDR 04, 2004 Software Defined Radio Technical Conference*. http://sdrforum.org/pages/sdr04/4.3%20Transmit-Receive%20Systems%201%20Chuprun/4.3-1%20Ahmed.pdf.

[45] United solar ovonic. *web site*, 2007. http://www.uni-solar.com.

[46] A.B. Smolders and G.W. Kant. System specification THEA. *web document*, 1999. www.astron.nl/ska/archive/technical/thea_spec.pdf.

[47] D. Thompson, R. Bairavasubramanian, G. Wang, N.D. Kingsley, I. Papapolymerou, E.M. Tenteris, G. DeJean, and R.L. Li. Microstrip antenna arrays on multilayer lcp substrates. *web document*, 2007. http://www.techbriefs.com/content/view/1098/34, LEW17980-1.pdf.

[48] S. Kayali, G. Ponchak, and R. Shaw. GaAs MMIC reliability assurance guideline for space applications. *JPL publication 96-25*, 1996. http://parts.jpl.nasa.gov/mmic/.

[49] Xilinx, Inc. Aerospace and defense. *web site*. http://www.xilinx.com/products/silicon_solutions/market_specific_devices/aero_def/index.htm.

[50] Xilinx, Inc. Xilinx product selection guides. *web document*, 2007. http://www.xilinx.com/publications/matrix/hirel_color.pdf.

[51] International Rectifier, Inc. RAD-Hard logic level MOSFETS. *web site*, 2007. http://www.irf.com/e/rhllfdenaus.html.

[52] Inc. Perkin Elmer. Rubidium time standards. *web site*, 2007. http://optoelectronics.perkinelmer.com/catalog/Category.aspx?CategoryName=Rubidium+Standards.

[53] L.E. Mosher S. Wiley, G. Herbert. Design and development of the near propulsion system. *Aerojet, Sacramento, CA, Johns Hopkins University*, 1995. http://near.jhuapl.edu/PDF/PS.PDF.

[54] J.E. Marsden and S.D. Ross. New methods in celestial mechanics and mission design. *Bull. Am. Amth. Soc.*, 43:43–73, 2006. http://www.ams.org/bull/2006-43-01/S0273-0979-05-01085-2/home.html.

[55] B.W. Adams. Apophis. *web site*. http://www.bernhard-adams.com/apohis.html.

[56] C. Hirata. Rockets and space transportation. *web document*, 2007. http://www.pma.caltech.edu/~chirata/deltav.html.

[57] J. Horsewood. 99942 apophis rendezvous mission opportunities. *SpaceFlightSolutions*, 2006. http://www.spaceflightsolutions.com.

[58] The space elevator reference. *web document*, 2007. http://www.spaceelevator.com/archives/2007/07/.

[59] P. Pempie and H. Vernin. Reusable expendable launcher cost analysis. *AIAA/ASME/SAE/ASEE Joint Propulsion Conference, Huntsville, AL, July 16-19 2000*, 2000. http://www.aiaa.org/content.cfm?pageid=406&gTable=mtgpaper&gID=6157.

[60] JPL. Jpl small-body database browser. *web applet*, 2007. http://ssd.jpl.nasa.gov/sbdb.cgi?sstr=99942;orb=1.

[61] Univ. of Michigan. Look out: Asteroid's near-miss may be home run for scientists. *press release on the web*, 2005. http://www.umich.edu/~urecord/0506/Sept06_05/10.shtml.